7

Quaderni del CAMIlab

Laboratory Physical Model

for infiltration processes modeling, landslides triggering and propagation

Edited by

Giovanna Capparelli

Pasquale Napoli

Gennaro Spolverino

Pasquale Versace

Laboratory of Environmental Cartography and Hydraulic and Geological Modeling

UNIVERSITÀ DELLA CALABRIA

Lab. di
Cartografia
Ambientale e
Modellistica Idrogeologica
UNIVERSITÀ DELLA CALABRIA

Quaderni del CAMIlab

Periodical publication by

Laboratory of Environmental Cartography and Hydraulic and Geological Modeling
Università della Calabria - Director : *Prof. Eng. Pasquale Versace*

Centre of Competence of the Italian Civil Protection for hydraulic and geological hazards (Decreto del 26.01.2005 emanato ai sensi della Direttiva del 25.02.2004)

87036 Arcavacata di Rende (CS) – Ponte P. Bucci cubo 41/B

Phone 0984 496 621/592/617 Fax 0984 496619

www.camilab.unical.it camilab@libero.it

Year 5 Number 7

July 2018

edited by
Giovanna Capparelli
Pasquale Napoli
Gennaro Spolverino
Pasquale Versace

Editing
Pasquale Napoli
Gennaro Spolverino

This book was made in collaboration with
Interuniversity Consortium for Hydrology

CINID
CONSORZIO INTERUNIVERSITARIO PER L'IDROLOGIA

Laboratory Physical Model

for infiltration processes modeling, landslides triggering and propagation

Giovanna Capparelli
Pasquale Napoli
Gennaro Spolverino
Pasquale Versace

For the physical model described in this manual we are indebted to the commitment and decisive collaboration of friends at the Università degli Studi della Campania Luigi Vanvitelli,

Professors

Emilia Damiano, Roberto Greco and Lucio Olivares.

With them we gladly share all the results attained to the present day and will work for further enhancement of the system.


Cameras

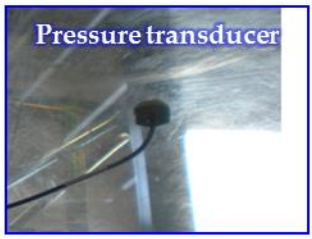
Pressure transducer


Spray nozzles

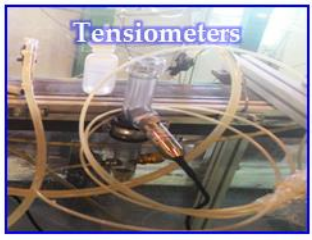
Tensiometers


Rain gauge


Laser


TDR

SUMMARY

INTRODUCTION

To reproduce and investigate the behavior of rainfall-induced landslides, tests can be performed in situ or laboratory analyses can be developed with physical scale models. The latter are based on the reproduction of the physical characteristics of the phenomena in question and the boundary conditions that control their dynamics. There are various configurations, which differ essentially in size, in the instruments installed and in their intrinsic performance potential.

Physical models have been widely used to analyze landslides (Iverson and LaHusen, 1989; Eckersley, 1990; Spence and Guymer, 1997; Wang and Sassa, 2001; Okura et al., 2002; Lacerda et al., 2003; Olivares et al., 2009). Besides having evident scientific utility, such scale models are particularly useful for all those cases which are difficult to monitor with instruments, since they make it possible to observe behavior that results in failure and the transient phases that precede it.

The schemes most commonly used are those which reproduce the typical scheme of the infinite slope and, thanks to a suitable sensor system, control various measurements required to understand the phenomenon, such as suction, the degree of saturation, and small displacements. The possibility of creating and setting up large physical models enables larger soil volumes to be analyzed and more faithful reproduction of the natural phenomenon, while minimizing boundary effects.

With this in mind, at the CamiLab laboratory of the University of Calabria, in the framework of the SILA – PONa3_00341 project An Integrated System of Laboratories for the Environment – a large artificial channel was built, able to reproduce a rainfall-triggered landslide, analyze the correlated measurements, and observe post-failure evolution.

The physical model was designed so as to lend the channel great flexibility and versatility when used. It is equipped with a sensor system to measure the main physical parameters which govern deformation and failure processes, a video recording system, lasers to measure displacements and devices to measure the velocities involved. The presence of two independent channels also makes it possible to analyze the propagation phase and allow the positioning of impact structures so as to evaluate any mitigation strategies.

The sections below report a detailed description of the scale model, including the mechanical component, the whole sensor system with its use and calibration, and a brief summary of a test and the results achieved.

PART 1

1. DESCRIPTION OF THE DEVICE

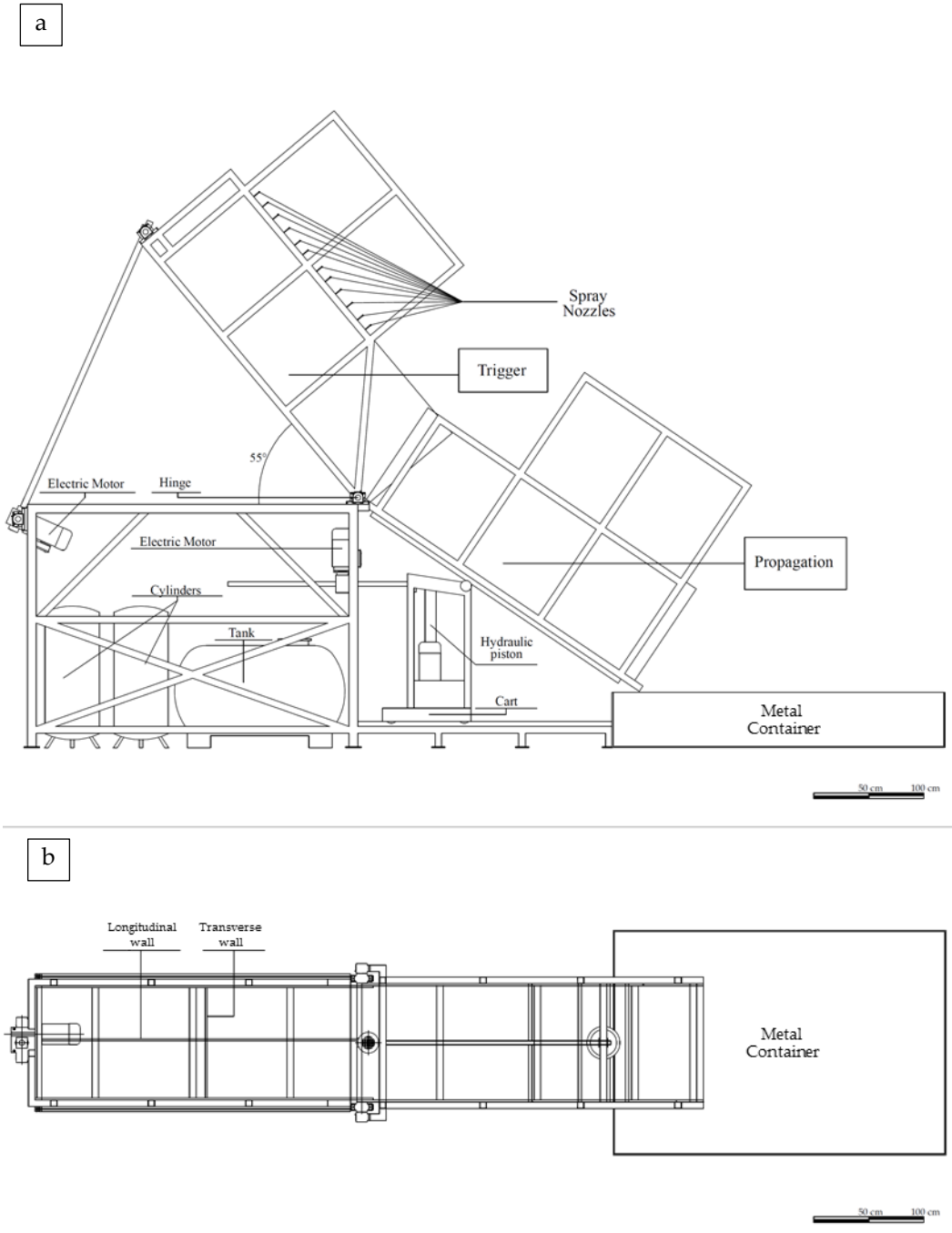

Figure 1: The physical model a) Section b) Plan.

1.1. MECHANICAL COMPONENT

The channel has a rectangular section which is homogeneous and constant along its entire length. The structure, supported by metal tubes, is 1 m high, 6 m long overall, divided into 3 m for the trigger and 3 m for propagation, and 1 m in width.

The section and plan of the mechanical component of the structure are reported in Figure 1, while Figure 2 shows two photographs of the side and front view of the channel. In the upper flume, drainage channels are installed which collected the water dripping from the side walls, and dividing walls may be installed, arranged longitudinally and vertically to the axes. This not only allows small study plots to be constructed but also tests to be carried out in parallel (Figure 3).

Figure 2: Physical model: a) Side view b) Frontal view.

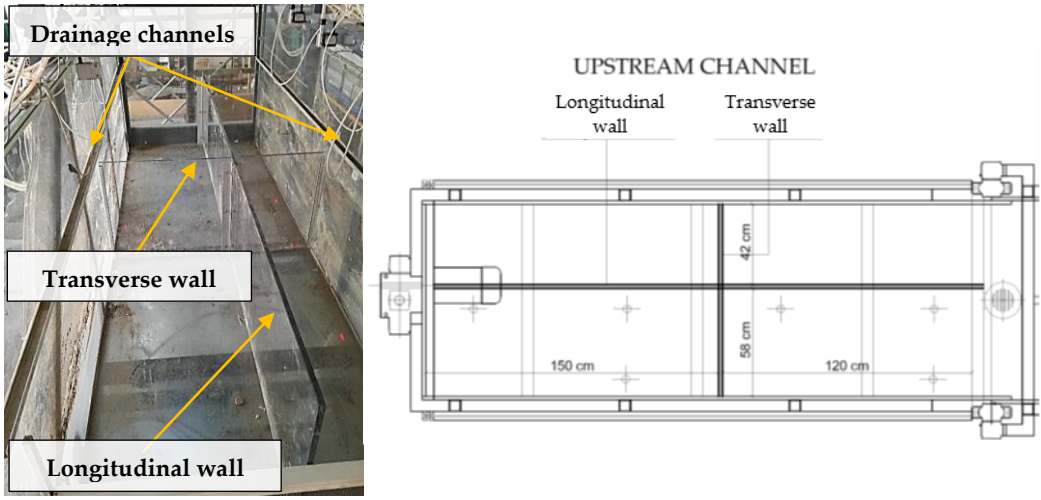

Figure 3: Detail of the upper flume, with longitudinal and cross dividing walls.

Both the side walls and the bottom wall are made out of transparent plexiglass panels to ensure that movement can be both viewed and filmed during the landslide. On the flume bed it is possible to reproduce both an impermeable and permeable bottom-base. In the former case, an impermeable rough bed is laid, which acts as an interface with the test soil, consisting of a plastic sheet on which gravel grains are glued; in the latter case, a permeable geotextile or geonet is used.

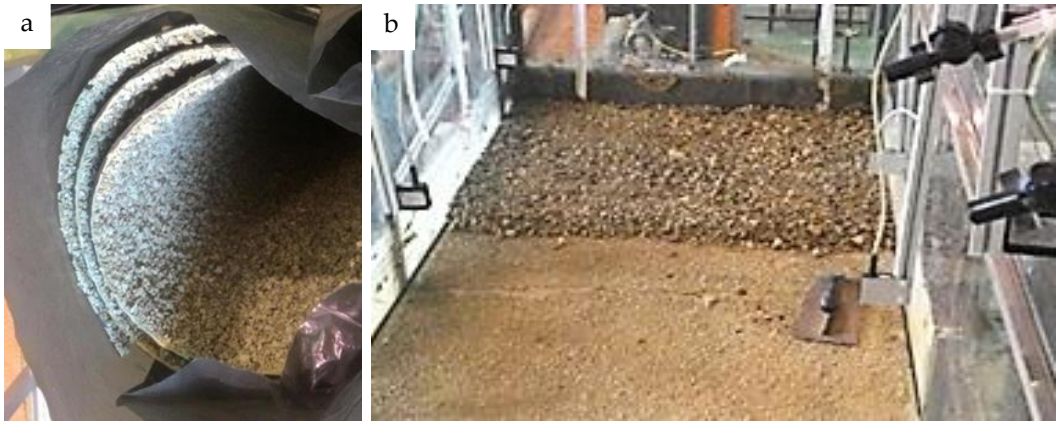

Figure 4: a) Impermeable rough bed. b) Laying the material on the impermeable bed.

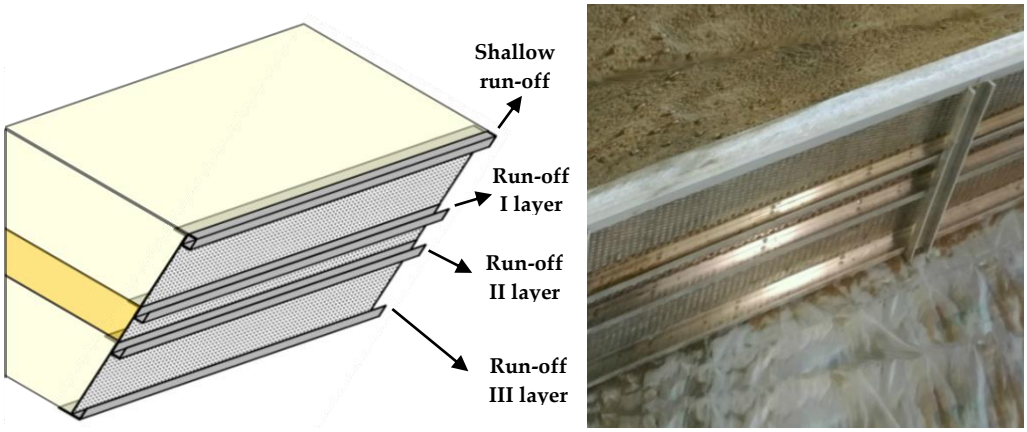

Figure 5: Draining grid laid at the foot of the slope with the water collection channels installed to measure run-off.

To hold the deposit a draining grid is laid at the foot of the reconstructed slope. Grids of different heights can be inserted according to the thickness of the reconstructed deposit. The grid is formed by a perforated metal sheet, on which a permeable geotextile is placed which permits drainage. Moreover, on the front part of the grid, transversal to the slope, small water collection channels can be mounted to measure both the surface runoff and the runoff from the individual soil layers. Figure 5 shows an example of a three-layer grid for a test, with installation of small channels to measure flows.

Artificial rainfall was applied with a 24-nozzle water particle sprinkler system, fed by a main 1000-liter tank and four 200-liter auxiliary tanks. The rainfall system integrates four pressure sensors and three auxiliary rain gauges. The arrangement of the nozzles was optimized so as to ensure rainfall uniformity, and minimize surface erosion and interference with the video system.

The pressure range varies between 0.1 and 7 bar with an intensity that can vary according to the nozzles used. The maximum variation, for each nozzle, ranges from 0.28 to 6.13 mm/h on 3 m^2. In addition to the artificial rainfall system, further acquisition systems are installed which permit data collection with a series of sensors for a total of 48 channels from tensiometers, pressure transducer, laser sensors to detect the soil level, auxiliary sensors (slope and pressure) and rain gauges.

The individual sensors are placed in various positions and each may be positioned to operate on various measurement configurations and

simulations. Finally, a series of motorized activation and control systems were installed, including pneumatic and hydraulic controls (Figure 6):

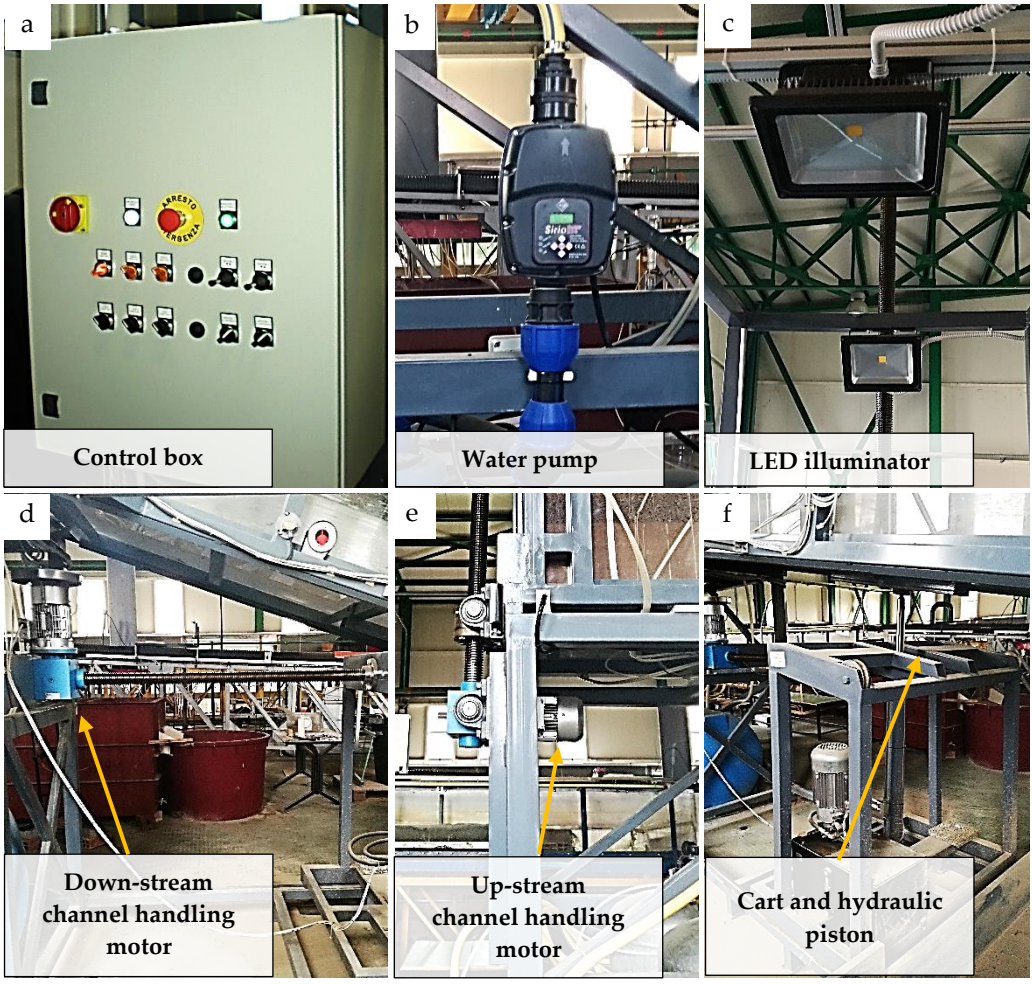

Figure 6: a) Electric control panel for channel movement and lighting and pump controls. b) Water pumping system for loading pressurized tanks. c) LED illuminators. d) e) Downstream and upstream channel handling motors. f) Cart for downstream movement and hydraulic control unit for widening the flume angle.

- electric control panel for channel movement and light and pump controls;
- water pumping system for loading pressurized tanks;
- lighting system with six LED illuminators;
- system of motors with reducers and jacks for channel movement;

- hydraulic control unit for widening the angle of the down flume;
- a series of sensors and auxiliary switches for the whole system.

The 48-channel acquisition system (Figure 7) is based on a "dedicated" PC, serially connected to:

- a box based on an NI acquisition card;
- a series of DSI data acquisition stations.

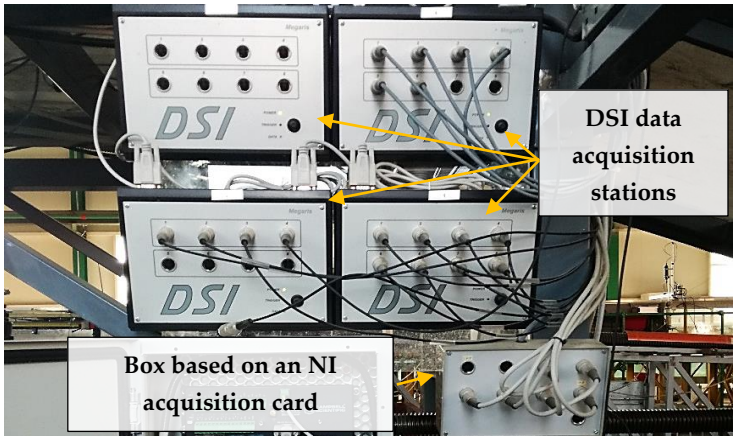

Figure 7: Acquisition stations.

1.2. SENSOR SYSTEM

The instrumentation in the artificial channel is able to measure the main parameters that control the physical phenomenon, thanks to the installation of the following equipment:

- Tensiometers (used to measure suction);
- Pressure transducers (used to measure pore water pressure);
- TDR device (used to measure soil water content);
- Rainfall system (used to simulate rainfall);
- Laser sensors (used to measure the soil profile and u_z displacements[1]);
- High-resolution video cameras (used to measure displacements along u_x and u_y[2]).

Figure 8 shows the sensors listed above their relative position along the structure. This sensor system is essential for measuring and monitoring the main parameters which control and regulate the phenomenon of landslides triggered by rainfall infiltration.

[1] They represent the displacements in orthogonal direction.

[2] They represent the displacements in directions x and y (in plan).

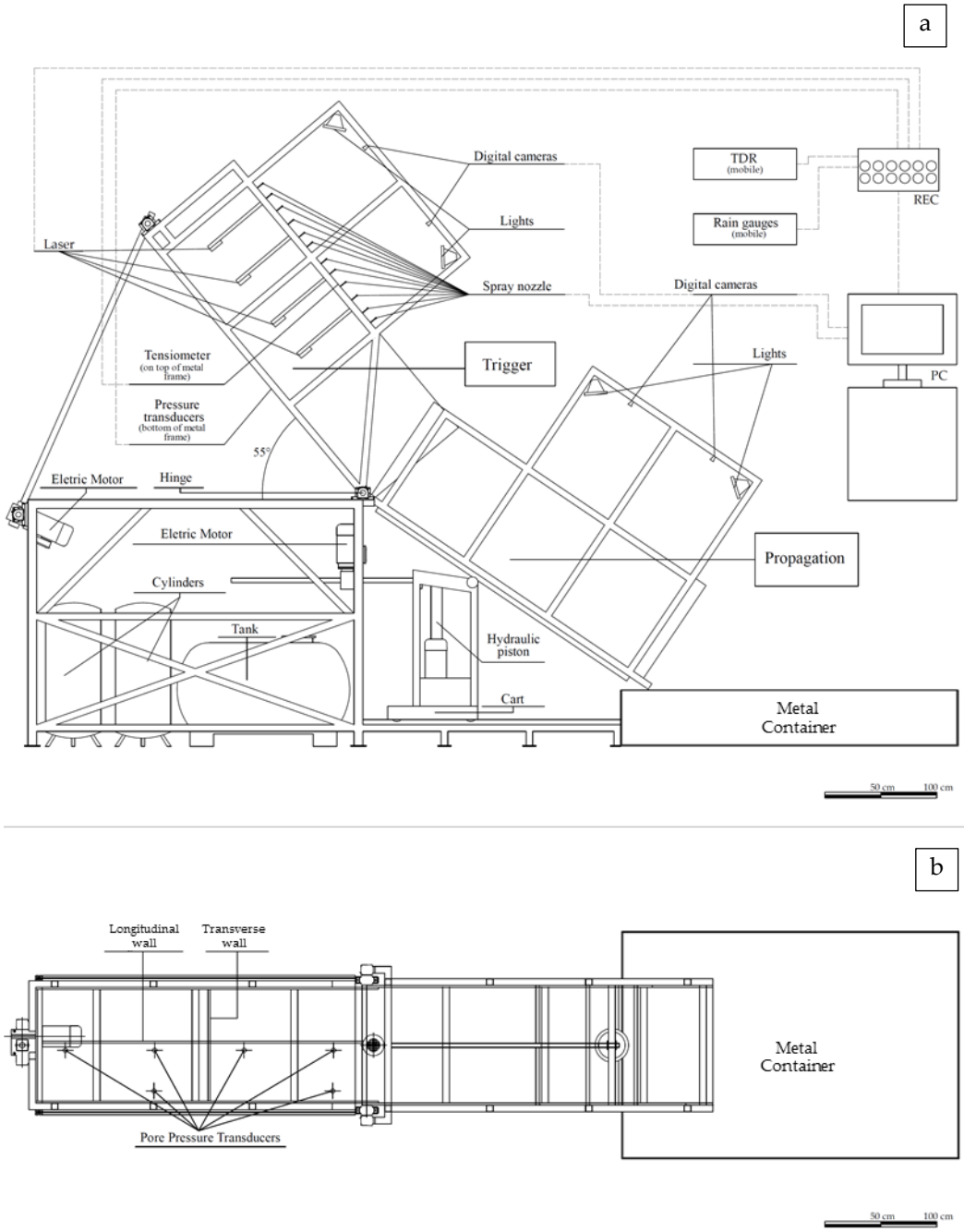

Figure 8: The physical models and sensor system: a) Section b) Plan.

A more complete scheme of the instrumentation with its main properties is reported in Table 1.

Measurement	Device	Manufacture/Type	Sensor	Sensor size		Transducer	Operating range	Linearity	Hysteresis	Output	Sampling Frequency
				Diameter	Height						
Matric suction	Tensiometer	Soil Moisture Corp/2100F	Porous ceramic cup	6 mm	25 mm	Current Transducer	0 - 100 Pa	0.0025	< 1%	4 - 20 mA	750 Hz

Measurement	Device	Manufacture/Type	Sensor	Sensor Probe size		Time Response of Combined Pulse Generator & Sampling Circuit	Maximum spatial resolution		Operating temperature range	Timing Resolution
				Diameter	Length					
Water content	TDR Apparatus	TDR100 Campbell Scientific	Small Probe	2 mm	75 mm	≤ 300 ps	1 cm a $\theta = 0.1\ m^3/m^3$	2 cm a $\theta = 0.2\ m^3/m^3$	−40 /55 °C	12.2 ps
			Medium Probe	3 mm	150 mm	≤ 300 ps	2 cm a $\theta = 0.1\ m^3/m^3$	4 cm at $\theta = 0.2\ m^3/m^3$	−40 /55 °C	12.2 ps
			Large Probe	5 mm	300 mm	≤ 300 ps	4 cm a $\theta = 0.1\ m^3/m^3$	8 cm at $\theta = 0.2\ m^3/m^3$	−40 /55 °C	12.2 ps
			Home-made probe	2.2 mm	80 mm	≤ 300 ps	1 cm a $\theta = 0.1\ m^3/m^3$	2 cm at $\theta = 0.2\ m^3/m^3$	−40 /55 °C	12.2 ps

Measurement	Device	Manufacture/Type	Sensor	Housig size (L - W - H)	Mesuring range	Resolution	Linearity	Output	Operating temperature	Sampling Frequency
Vertical displacement	Sensor displacement	LCL 45/100 - fae	Laser CMOS - array	62 mm -17 mm - 50 mm	100 mm	0.03 %	± 0.2%	4 - 20 Ma (analogic)	−10 /60 °C	Lens C-Mount High Res

Measurement	Device	Manufacture/Type	Sensor	Housig size (L - W - H)	Frame rate	Resolution	Pixel size	Video Output	Image Area	Power consumption
Displacement ux - uy	Digital Camera	Basler/ICX445	1/3" progressive	42 mm - 29 mm - 29 mm	22 fps	1296 da 966	3.75 µm - 3.75 µm	YUV 4:2:2 Mono - Bayer	100 cm by 150 cm	2.5 W (PoE) 2.2 (AUX)

Accessory: Obiettivo C-Mount High Res - 1/2" - 4 mm - F/1.4 w/lock Basler Digital I/O cable with HRS 6-pin connector, 10 m Mega–Pixel Lens Fixed FL 8 mm - 2/3" - f/1.1 - f/16

Measurement	Device	Manufacture/Type	Sensor	Sensor size		Operating range	Resolution - Accuracy	Operating Temperature	Output	Compensated temperature
				Diameter	Height					
Pore water pressure	Pore pressure transducers	TE Connectivity Measurement Specialties	SENSOR 2PSIG 1/2NPT .5-	12.7 mm	25.4 mm	0 - 13.79 kPa	0.3 % - ± 1%	− 20 /70 °C	0 - 5 V	0 - 40°C

Measurement	Device	Manufacture/Type	Sensor	Sensor size		Operating range	Resolution	Maxiumum temporal Resolution
				Diameter	Height			
Rainfall intensity	Rain gauge	Oregon Scientific PCR800	Tiping bucket	87 mm	107 mm	0 - 999 mm/h	1 mm/h	1 min

Table 1: Main characteristics of devices.

1.2.1. TENSIOMETERS

Suction is measured with a series of small-tip tensiometers (model 2100F – Soilmoisture Equipment Corp.).

The body is formed by a transparent plastic rigid tube on which a capsule is lodged for air circuit bleeding as well as an automatic acquisition transducer. The ceramic porous tip, 2.5 cm long and with a diameter of 6 mm, with a nominal air entry value of 100 kPa, is connected to the tensiometric body by means of a capillary tube protected by an external nylon tube 2 m long (Figure 9). The tensiometers are installed in the soil and their functioning is based on the interaction of equilibrium between the porous ceramic cap filled with water and the surrounding soil. When the soil that surrounds the bulb is saturated, the transducer indicates zero. The more the soil dries out, the higher the matrix potential becomes, and the water content in the instrument comes out through the porous bulb outside it. The transducer then indicates progressively growing values of depression.

These type of tensiometers are unable to measure matrix potentials greater than 1 bar. Indeed, the range of suction measurement varies between 0 and 100 cb. The model of tensiometer used considerably simplifies both installation and saturation operations, the latter being indispensable for the sensor to work properly.

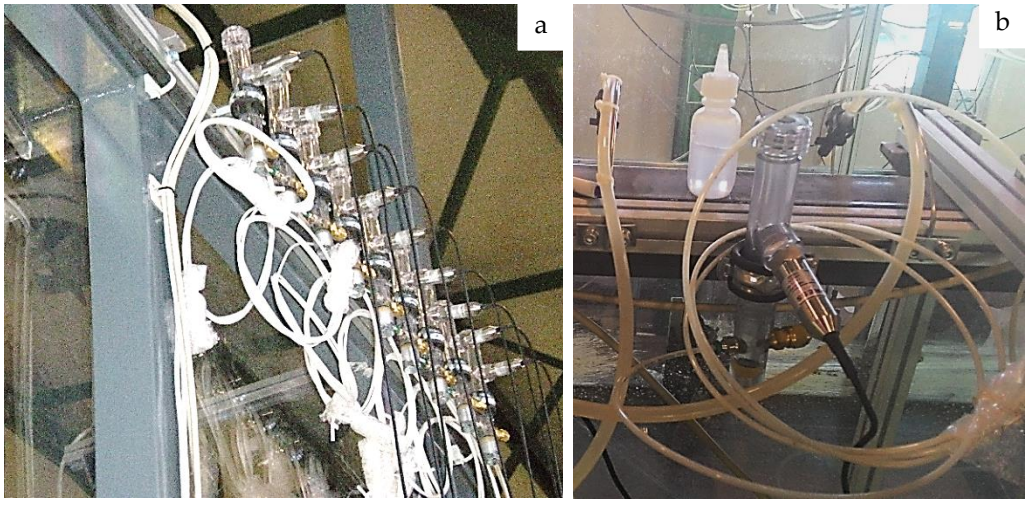

Figure 9: a) Tensiometers installed on the channel structure. b) Detail of a tensiometer.

Indeed, it is sufficient to fill the tank, thanks to the use of a simple manual pump, and remove all the air accumulating in the instrument, proceeding both from the vent tube, and using a depression on top.
In soft soils, as are easily encountered on test soils, tensiometers are installed by inserting the porous cap at the set depth. It is necessary for the operation to be performed in such a way that there is minimum disturbance to the soil. After installation, to avoid the surface water flowing into the hole along the tube, it will be appropriate reconstruct the deposit by filling better and accurately the hole produced by inserting the device. After installation, to be able to read correct suction values, it will be necessary to wait for the tensiometers to stabilize, i.e. for the equilibrium to be reached between the porous cap and the surrounding soil. This interval is due to the disturbance caused to the soil by the installation procedure: the drier the soil, the longer the interval. Once this initial period is past, the suction values will be able to be measured with great accuracy, and their variations can be monitored in almost real time.

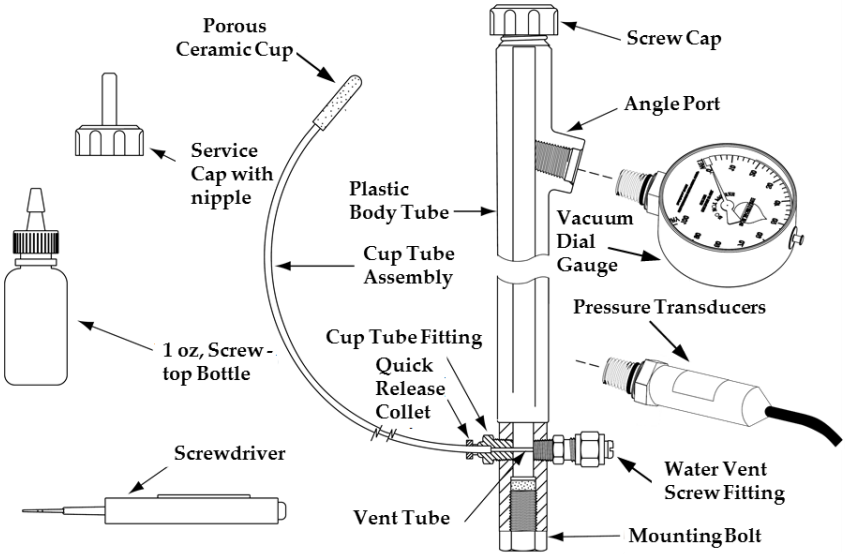

Figure 10: Tensiometer parts.

Pressure transducers are installed on the tensiometers, linked to SDI acquisition systems which allow the process to be automated and the data to

be stored in a data logger. To determine the measurements of interest, use is made of dedicated software, with which the acquisition frequency can be chosen. To eliminate any instrument errors, each tensiometer should be appropriately calibrated. Calibration consists in comparing pressures recorded by the sensor with different pressures applied. The porous caps are inserted within a graduated beaker full of water, positioned at a lower height than the transducer and the applied pressure is noted, i.e. the difference in height between the water free surface within the beaker and the sensor. The values recorded by the tensiometer are acquired in various configurations, making the pressure applied vary on each occasion. Thus different applied pressures are obtained with the relative values recorded and, by including such values in the system, it is possible to construct a regression curve which associates recorded values with actual pressures.

Applied pressures	
[cm]	**[kPa]**
-75	-7.5
-87.5	-8.75
-100.5	-10.05
-114	-11.4
-125.5	-12.55
-138.5	-13.85
-149.5	-14.95

Table 2: Applied pressures

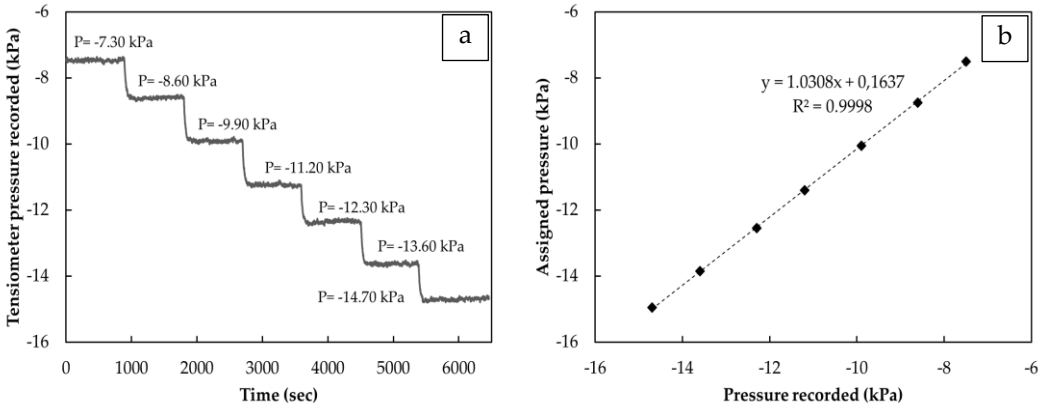

Figure 11: Example of calibration of a tensiometer. a) The graph shows the recorded response, in terms of pressure values, of the instrument at the various pressures applied. b) The graph shows the calibration curve of the tensiometer used.

An example of calibration of a tensiometer installed on the artificial channel is reported in the Figure 11 and Table 2. Table reports the various pressures applied, while Figures 11 a/b show respectively the pressures recorded by the instrument and the calibration curve obtained with a linear regression.

1.2.2. PRESSURE TRANSDUCERS

A pressure transducer measures the pressure of a liquid or gas by means of an electric signal sent to a receiver in analog format. Neutral pressure transducers are used to measure neutral positive pressures and monitor excess pressures induced by slope failure in the course of tests. The principle is based on the physical strain gage deformation present in the transducer membrane: electrical resistance is proportional to the applied pressure, which is translated into an electric signal. The transducers considerably simplify the procedure of processing and recording data since the electric signal from the transducer can be digitalized and sent to a computer. This characteristic has led in time to adopting transducers instead of conventional manometers, also in measuring stationary pressures, especially when many pressures have to be measured. The model of transducers installed (LM31-00000F-2 PSIG - TE Connectivity Measurement Specialties) is a stainless steel sensor with PVC isolating connector (Figure 12).

The transducers are specially lodged on the channel bottom and have to be saturated prior to the soil layer being placed. The membrane is protected by a porous plate which prevents the inclusion of soil particles. The operative pressure for the series in question is 13.79 kPa (2PSI) with the maximum pressure of 137.9 (20PSI). Precision is ± 0.3%, the total error range ± 3%, and the working temperature is -20 / 70 °C. The pressure transducers must also be calibrated. The procedure is fairly straightforward and consists in applying above the load cell a water column of known height and record the output signal from the sensor once it has stabilized. The applied pressure value is thus obtained with the respective measured pressure value. By varying the height of the water column, we may obtain a series of values which, if fitted with linear regression, supply the calibration curve.

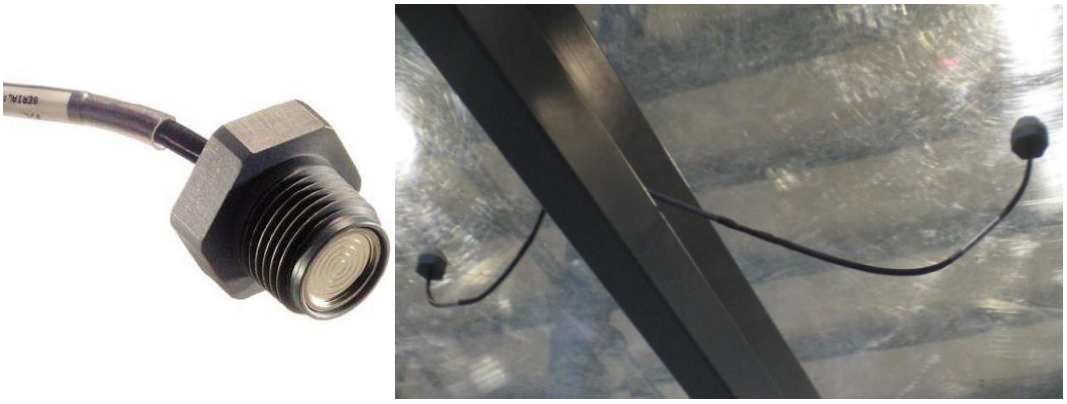

Figure 12: LM31-00000F-2 PSIG pressure transducers installed on the flume bed.

Pressure applied	
[cm]	[kPa]
0	0
9	0.9
12	1.2
15	1.5
21	2.1

Table 3: Pressure values applied.

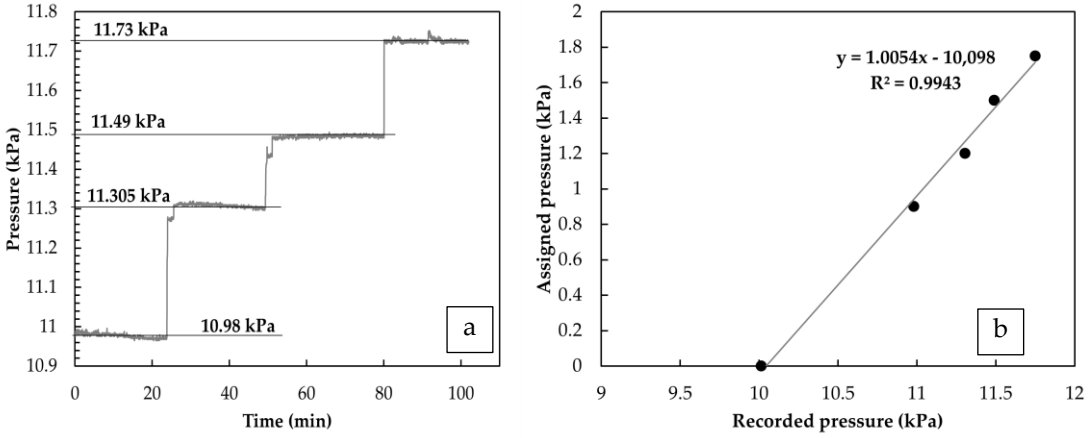

Figure 13: Example of calibration of a pressure transducer. a) The graph shows the recorded response, in terms of pressure values, of the device at the various pressures applied. b) The graph shows the calibration curve of the transducer used.

An example of calibration of a pressure transducer installed on an artificial channel is reported in the Figure 13 and Table 3. Table reports the various pressures applied, while Figures 13 a/b show, respectively, the pressure values recorded by the instrument and the calibration curve obtained with linear regression.

1.2.3. TDR Device

Time domain reflectometry (TDR) is one of the most widely used techniques to measure soil water content and electrical conductivity both for laboratory tests and for field measurements (Dasberg & Dalton, 1985; Topp & Davis, 1985; German et al., 1997; Greco, 2006). It can be used to determine volumetric water content (θ) indirectly, insofar as the probes do not measure explicitly the quantity of water found in the soil, but determine its relative dielectric constant (ε_r). The technique is based on measuring the time taken by an electromagnetic wave to cross a metal probe immersed in the soil. The wave propagation velocity (V_P) depends on the soil dielectric permettivity, which in turn depends on the quantity of water present in the sample. The measurement system is illustrated in Figure 14 and comprises a datalogger connected to a system consisting of a generator of rectangular pulses and an oscilloscope connected to a multiplexer, to which eight probes can be connected.

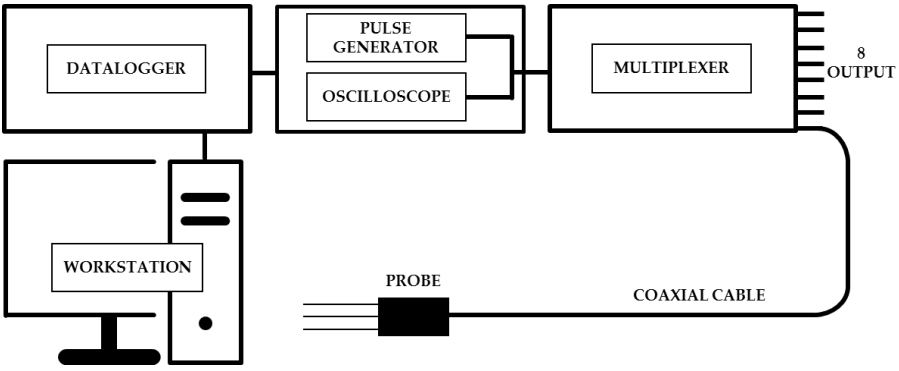

Figure 14: TDR device.

The instrument on the channel consists in a TDR100-based Campbell Scientific System connected to various types of probes of different size. Moreover, "home-made" TDR probes were also constructed with the same shape as those already installed, but with a preference for smaller size

(Figure 15). Smaller probes allow better point-based water content measurements to be obtained and the soil is less disturbed. All the types of probes are produced with three metal rods, i.e. the optimal number, insofar as, by adopting more rods, there is little improvement in results (Zegelin et al., 1992).

The probes may be arranged either horizontally or vertically. The choice is made according to the stratigraphy of the soil in question.

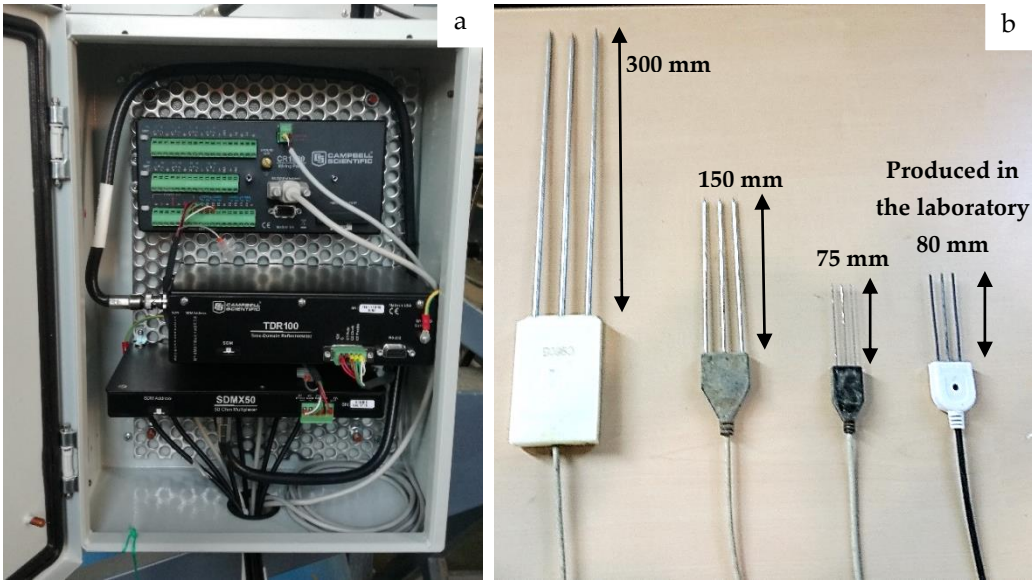

Figure 15: a) Multiplexer and TDR100 reflectometer controlled by the datalogger. b) TDR probes.

1.2.4. LASER DISPLACEMENT TRANSDUCER

The artificial channel, in order to monitor the displacements along the orthogonal profile, is equipped with triangulation laser sensors, model LCL45/100 U-485 BI5M. This measurement system is based on a simple geometric relation. A laser diode emits a laser ray that hits the measurement target. The reflected light ray is transferred through a lens to a matrix or vector (digital sensor) or point-based data (analogical sensor).

The intensity of the reflected beam depends on the reflective capacity of the object to be measured. The distance is determined with extreme precision, using simple trigonometric calculations with a lower resolution at fractions of a micrometer. Schematically (Figure 16):

- radiation of a laser semiconductor (1) is focused by a lens (2) on an object (6);
- the radiation reflected by the object is collected by a lens (3) on a linear CMOS array (4);
- a signal processor (5) thus calculates the distance from the object.

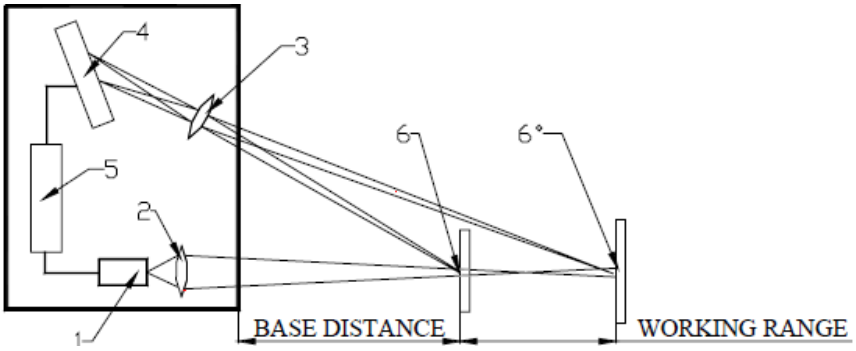

Figure 16: Operative scheme of laser system.

Laser point sensors are frequently used due to their simple operation and the ease of alignment with the target thanks to the visible laser spot target. Depending on the version, the optical principle allows measurement at distances exceeding 1 m, maintaining nonetheless a good field of precision. Depending on the accuracy required, there are versions available with very small, precise fields of measurement and gradually increasing fields of measurement, which nevertheless ensure high performance.

Figure 17: Laser sensor installed (model LCL45/100 U-485 BI5M).

For the model installed (Figure 17) excellent precision and resolution are also obtained in rapid measurements, due to the number of sensors installed (n = 6) and the good arrangement in the channel. Indeed, the measurement base is 45 mm with a working range of 100 mm and a resolution error 0.03%, as indicated in the technical data sheet accompanying the instrument.
In applications it is observed that the presence of water particles and roughness due to the soil produce a noise. Yet the latter is in some way acceptable insofar as it generates values which oscillate in the range of a tenth of a millimeter. The values measured by the laser during rainfall simulation are shown in Figure 18.

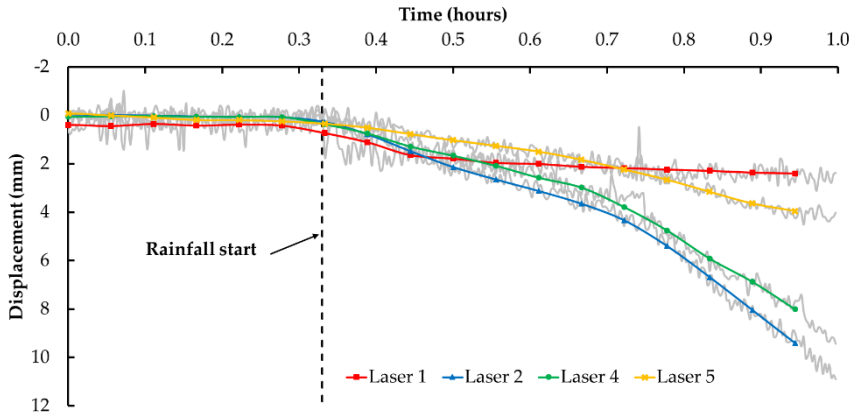

Figure 18: Pattern of displacements detected by the laser devices installed on the artificial channel.

After the start of rainfall, the laser devices record the growing displacement values which correspond to a lowering of the ground surface. As may be seen from the graph, the lowering reaches about a centimeter (laser 2).

1.2.5. IMAGE ACQUISITION SYSTEM AND PIV TECHNIQUE

Besides monitoring the displacements perpendicular to the surface of the deposit, it is also possible to know longitudinal changes, thanks to an image acquisition system with the relative dedicated particle image velocimetry (PIV) system. For image acquisition high-resolution (1296 x 966) video cameras (ICX445 – Basler) are used, with two positioned in the triggering zone, two in the propagation zone and two at the side of the channel, thanks to jutting metal supports. Two lenses are used with the video cameras

(C-Mount High Res - 1/2" - 4 mm - F/1.4 w/lock and Mega–Pixel Lens Fixed FL 8 mm - 2/3" - f/1.1 - f/16), as well as a 10-meter digital cable.
The dedicated PIV system permits optical evaluation of the flow domain of the deposit during the various test phases. It supplies, in a certain section, the projection of the field of instantaneous velocity.
From the comparison of the two successive images the velocity of the space-time relation is evaluated, in other words the pixels between the position of the same particle in two successive photos, and the acquisition time of the two photos. The laser device emits two pulses, separated by an interval Δt, which illuminate the particles and make them visible to the camera. By means of a synchronizer, the camera takes two photos when the signal is emitted by the laser. The two images undergo correlation processes whereby the movements of particles present in each area are compared (32x32 or 64x64 pixel measurement grid). The density of particles (>25 per window) ensures that correlation processes and average are satisfied. Indeed, such processes restore spatially averaged velocities within the measurement grid.

$$\bar{U} = \frac{\Delta x}{\Delta t}; \quad V = \frac{\Delta y}{\Delta t} \tag{1}$$

Using PIV acquisition software the images captured can be processed, correlating and validating the flow domain. To obtain values that are compatible with the real phenomenon, the choice of photogram acquisition frequency is decisive: the interval between two shots must capture the particles in the two consecutive images. Besides, also in the case of bidimensional flow, if the interval is too long, there is a loss of information between the two images and the velocity obtained can no longer be assimilated to instantaneous velocity, but is instead an average velocity. Instead, if the interval is excessively short the displacement is too small and the disturbance due to "noise" and the imperfect correlation between pairs of windows becomes dominant with respect to the real same displacement: a field of velocity is obtained which does not correspond the real one. The value of Δt will have to oscillate about ~10 μs. Hence the technique, through high-resolution image acquisition, allows us to recognize individual soil particles and detect the development of processes generated during the simulation. The output supplied by PIVview2C software can be obtained according to the format required and the size desired. Essentially, screen views are supplied with velocities and displacement values with the relative text files.

Below are two images reporting successive instants of a test with the results of the simulation using PIVview2C software. The first images concern the field of velocity, with the next showing images at saturation which present the displacement patterns.

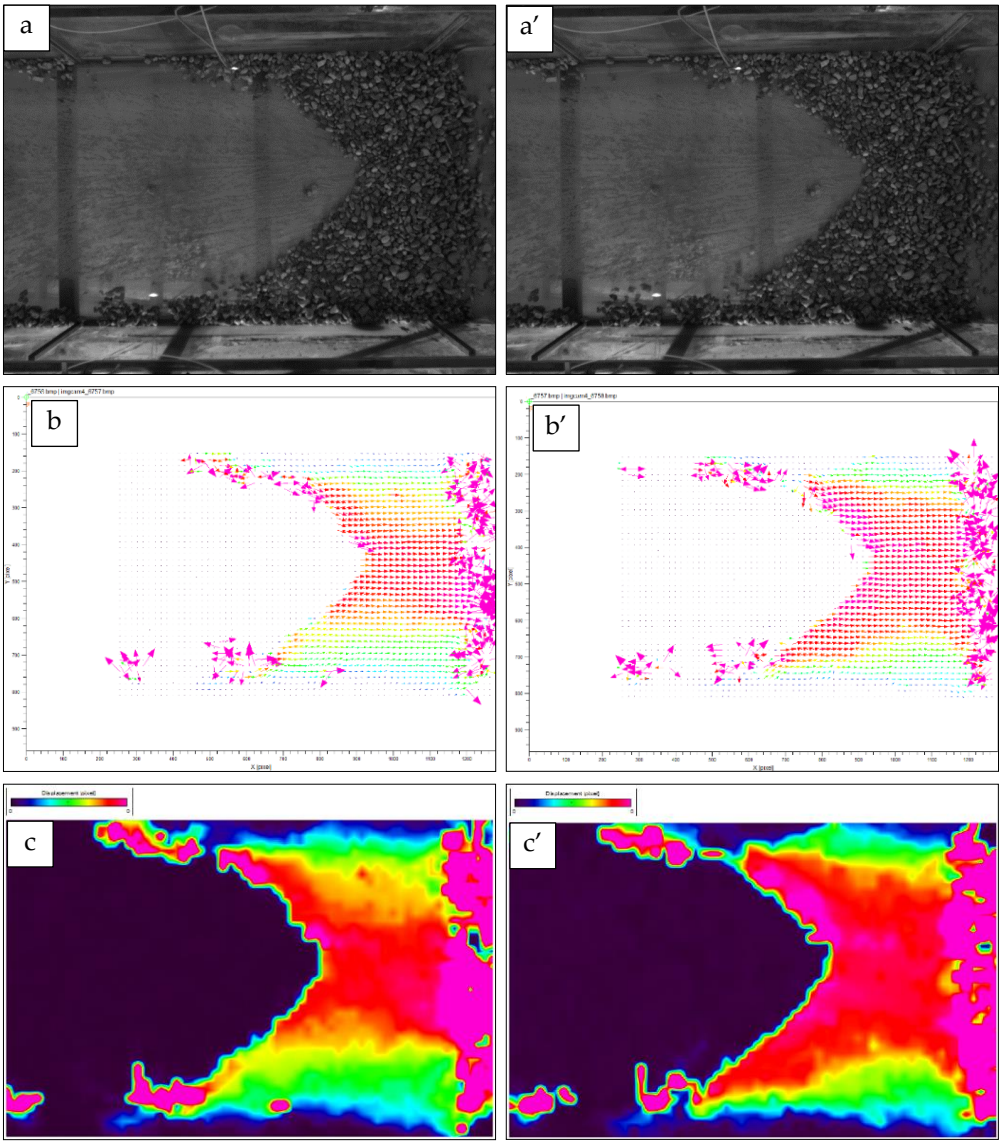

Figure 19: a) a′) Successive instants of a test. b) b′) Field of velocity. c) c′) Field of displacements.

1.2.6. RAINFALL SYSTEM

The system integrates a 24-nozzle rainfall simulator, the main 1000-liter tank and four 200-liter auxiliary tanks (Figure 20). The system has four pressure sensors and three rain gauges. Water flow is activated by four proportional valves (flow regulation) and four on/off valves (*duty cycle*). Separation into four circuits was introduced to offset the pressure variations due to the different height of the nozzles resulting from the trigger flume system. Especially at low pressures, the differences due to height significantly affect the uniformity of supply. Hence the subdivision into four circuits, which guarantees greater homogeneity.

Flows are monitored by pressure sensors and flow regulation is based on the control of pressure from a compressor and a tank outside the system. Regulation occurs through proportional valves directly on the four tanks. The on/off valves are positioned on the distributors and allow rapid activation and shut-off of supply to regulate the *duty cycle* and interrupt supply. The nozzles may be one of two types, either violet or orange, with different flows in relation to the different pressure.

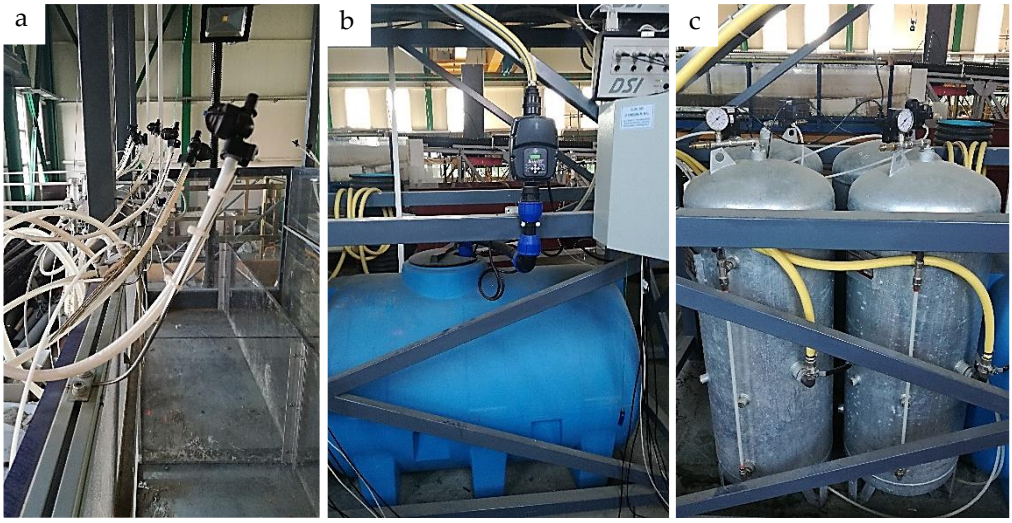

Figure 20: Rainfall system. a) Spray nozzles. b) Main tank. c) Auxiliary tanks with pressure regulation.

nozzles	Violet		Orange	
Pres. (kPa)	l/h	mm/h	l/h	mm/h
10	19.90	6.72	52.75	17.52
20	28.13	9.36	74.59	24.96
40	39.77	13.20	105.50	35.28
80	56.23	18.72	149.18	49.68
120	68.88	23.04	182.71	60.96
160	79.54	26.40	210.98	70.32
240	97.42	32.40	258.41	86.16
300	108.91	36.24	288.91	96.24
400	125.76	42.00	333.60	111.12
500	140.59	46.80	372.98	124.32
600	154.03	51.36	408.58	136.08

Table 4: Rainfall intensity vs. pressure.

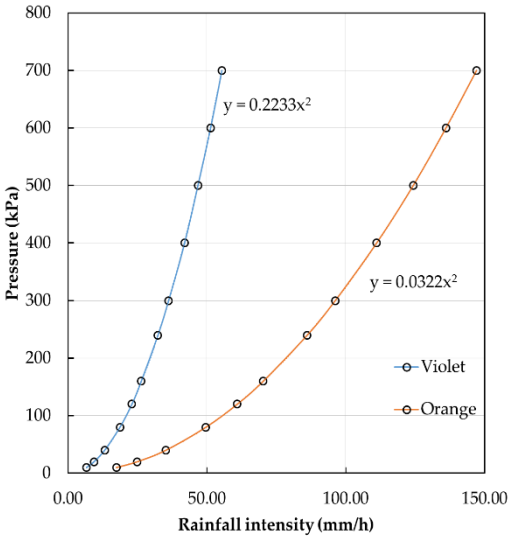

Figure 21: Rainfall intensity vs. pressure.

Table 4 and Figure 21 illustrate the relationship between flow and pressure; in particular the water flow from a single nozzle (violet or orange) is expressed both in l/h, and in equivalent mm/h on the surface of the entire upper flume, i.e. 3 m^2.

To regulate the flow in a broader range, *duty cycle* control is possible (partial activation in time) and/or total closure of some nozzles through taps situated at the various distributors. To regulate supply, four groups of each are connected to a collector equipped with a pressure sensor. It is thus possible to regulate the supply pressure from six nozzles independently so as to optimize flows at four different heights. The acquisition and control PC monitors the four pressure sensors and thus regulates the pressure on the four auxiliary tanks, controlling the discharge from the group of nozzles. Regulation occurs through proportional valves directly on the four tanks. The rainfall intensity used varies according to the physical model adopted and the reference hyetograph.

1.2.7. RAIN GAUGES

Rain gauges are used to measure and verify rainfall. To date, the system uses five rain gauges (model PCR800 – Oregon Scientific) connected to an acquisition system, which allows data to be recorded and automatically saved.

The rain gauge consists of a collection funnel and a tipping bucket connected to a magnet which activates a relay that, in turn, generates a pulse recorder by a counter. Each bucket is equivalent to 1.3 mm of rain.

When necessary, these instruments may be easily used to measure flows which are generated within the system. Indeed, if placed downstream of the system of collection channels, using tubes arranged to channel the water leaving the layers, they restore the surface and sub-surface flows. Figure 22 shows two rain gauges installed within the artificial channel, positioned to measure rainfall intensity.

Figure 22: Oregon Scientific PCR 800 rain gauge.

PART 2

2. INSTRUMENTAL SET-UP

2.1. USE AND CALIBRATION OF INSTRUMENTS

For proper interpretation of the results appropriate calibration techniques need to be set up and developed in advance. This section describes how the instruments installed on the physical laboratory model are to be used and the relevant procedures for their calibration.

2.1.1. TENSIOMETERS

The transducer, mounted on a tensiometer, has a field of measurement between -100 and 0 kPa. The tensiometers are installed in the reconstituted soil deposit, inserting the porous cap at a predetermined depth. Prior to installation the instruments must be maintained so as to ensure that the tensiometer is saturated and that the instruments are not damaged.

Attention should be taken not to damage the transducer and the ceramic tips during the unpacking and preparation phase. In particular, the ceramic tips should not come into contact with fats or other substances which could block their pores. After assembly, which should be done so as to ensure the that the device is watertight, the tensiometric body is then filled with distilled water and deaerated, keeping the ceramic tips immersed in water (Figure 23a).

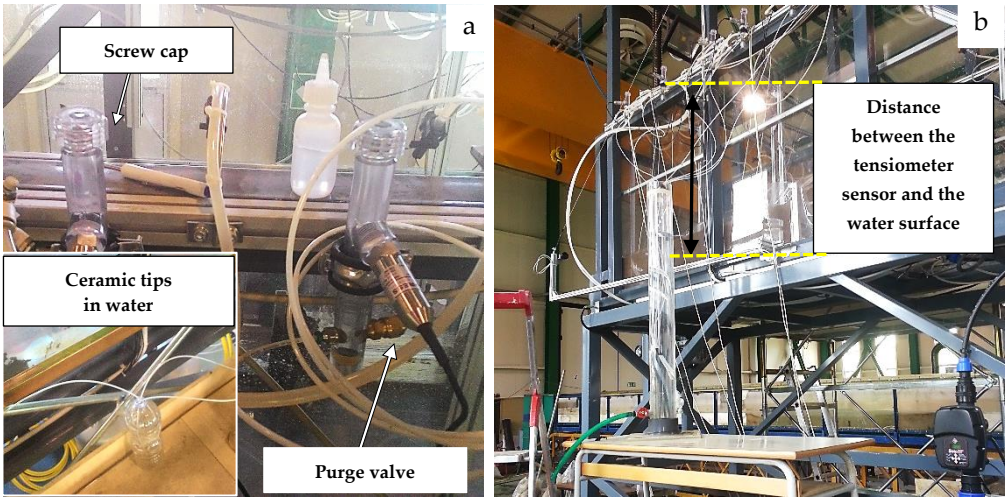

Figure 23: a) Tensiometer saturation phase. b) Calibration phase.

Having been filled, the spout of the bottle is placed full of water at the inlet of the purge valve, after removing the screw cap and, closing the spout at the

valve inlet, the bottle is tightened to apply pressure to the device, so as to saturate the connected tube and remove the air bubbles. The purge valve is then closed and with the same bottle a depression is made on the top to remove any other air bubbles.
The measurements performed during the test have to be adjusted for any difference in height between the device for measuring (ceramic tip) and reading (pressure transducer). After each test the instruments are once again maintained and the porous plates are kept in distilled water and deaerated until they are next used. It should be stressed that, should the desaturation of one or more instruments occur during a phase of evaporation or suction redistribution in soil with a very low water content, they should be drained prior to continuing with the test operations. In this case, the porous cap being in contact with the soil, the instrument is uninstalled, maintained and then reinstalled. Alternatively, only one operation is carried out: the tensiometer is filled with water and the water is pumped toward the cap on an open hydraulic circuit. This does not ensure the complete elimination of the air bubbles. Hence the next measurement could be subject to error. In the latter case, at the end of the test, if no further problems have arisen, the instrument needs to be recalibrated in the new condition.

2.1.1.1. TENSIOMETER CALIBRATION

The instruments are calibrated by keeping the tips immersed in water and by placing the body of the tensiometer and the measuring device at a known height above the tip so as to create a depression equal to the height of the water column at the head of the tip.
By varying the distance between the measuring point (porous plate) and the measuring device (pressure transducer), different suction values are induced (Figure 23b) which are recorded at one-second time intervals. The correlation between the values recorded and the applied suction supplies, for each instrument, zero and the calibration constant.
Figures 24 and 25 report (left) the recordings made by the tensiometers during the calibration procedure, and (right) calibration results, with the relative correlations identified. In the left-hand graphs, to each horizontal section there corresponds the measurement relative to each load applied (Table 5), while the sub-vertical sections indicate the phases in which the suction is varied, from which it is possible to deduce the response time of the instruments if the change in the load is applied almost instantly. In the

environmental conditions in which the calibration was conducted (t = 25°C) the precision of each tensiometer is about 0.1kPa.

Load applied		Tensiometers placed on the right-hand side of the flume					
		Tens. 1	Tens. 2	Tens. 3	Tens. 4	Tens. 9	Tens. 10
(cm)	(kPa)	(kPa)	(kPa)	(kPa)	(kPa)	(kPa)	(kPa)
-75.5	-7.55	-9.45	-7.65	-7.5	-7.65	-7.2	-6.7
-88.5	-8.85	-10.7	-8.9	-8.7	-8.9	-8.5	-7.9
-100	-10	-11.8	-9.95	-9.8	-10	-9.65	-9
-111.5	-11.15	-12.9	-11.1	-10.9	-11.1	-10.7	-10
-124	-12.4	-14.1	-12.3	-12.1	-12.35	-11.9	-11.3
-138	-13.8	-15.45	-13.7	-13.4	-13.6	-13.4	-12.5
-149.5	-14.95	-16.55	-14.8	-14.5	-14.95	-14.4	-13.6
Load applied		**Tensiometers placed on the left-hand side of the flume**					
		Tens. 5	Tens. 6	Tens. 7	Tens. 8	Tens. 11	Tens. 12
cm	kPa	[kPa]	[kPa]	[kPa]	[kPa]	[kPa]	[kPa]
-75	-7.5	-7.7	-7.1	-7.5	-8.35	-7.3	-7.8
-87.5	-8.75	-8.8	-8.3	-8.6	-9.5	-8.4	-8.9
-100.5	-10.05	-10.1	-9.65	-9.9	-10.8	-9.75	-10.2
-114	-11.4	-11.5	-11	-11.2	-12.1	-11.05	-11.5
-125.5	-12.55	-12.6	-12.1	-12.3	-13.2	-12.1	-12.7
-138.5	-13.85	-13.85	-13.3	-13.6	-14.5	-13.4	-13.9
-149.5	-14.95	-15	-14.4	-14.7	-15.6	-14.5	-15

Table 5: Correspondence between the loads applied and the loads recorded by the tensiometers during the calibration phase.

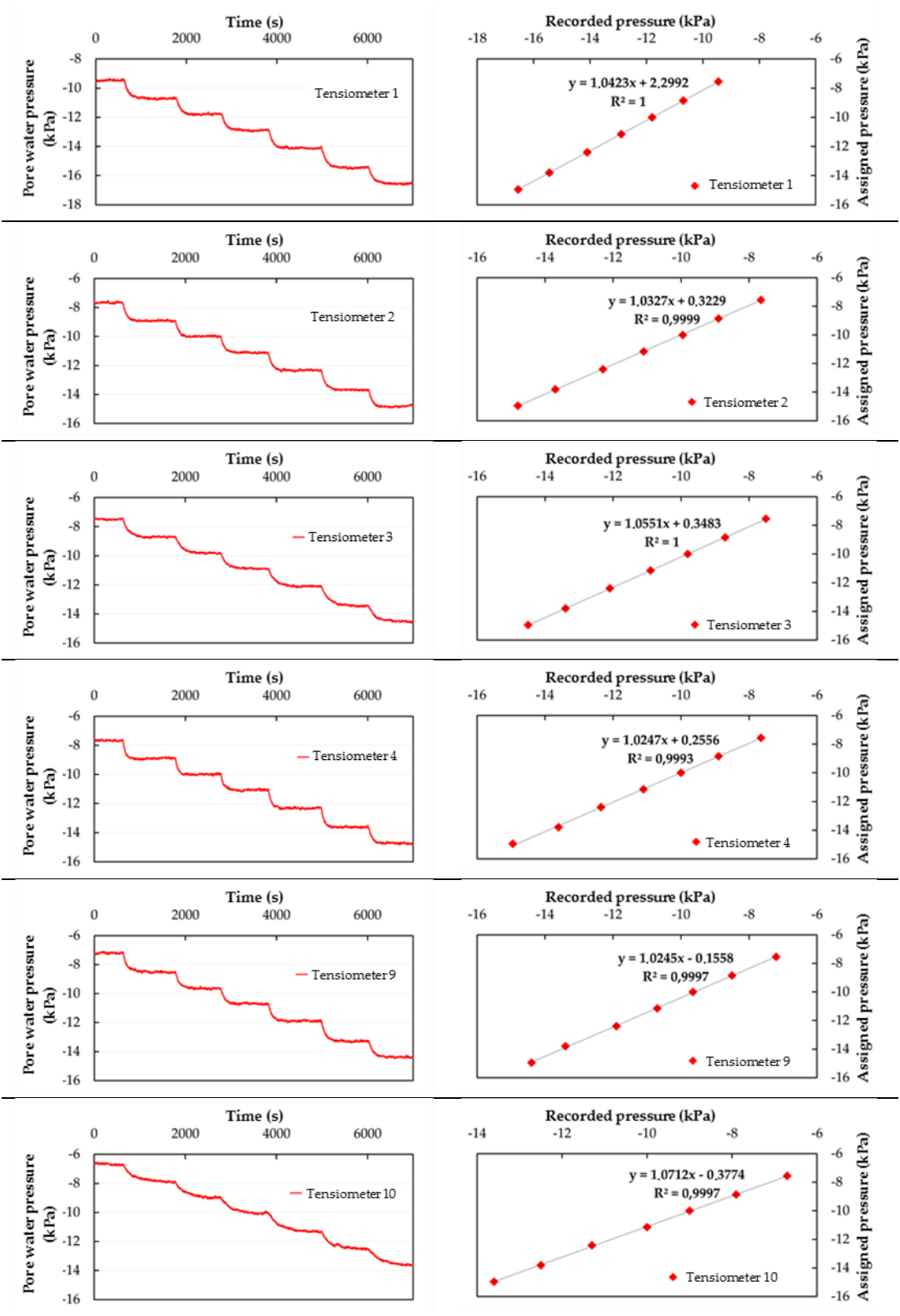

Figure 24: Right-hand graphs - Correlation between suction values applied and those recorded Left-hand graphs - Values recorded by tensiometers during calibration.

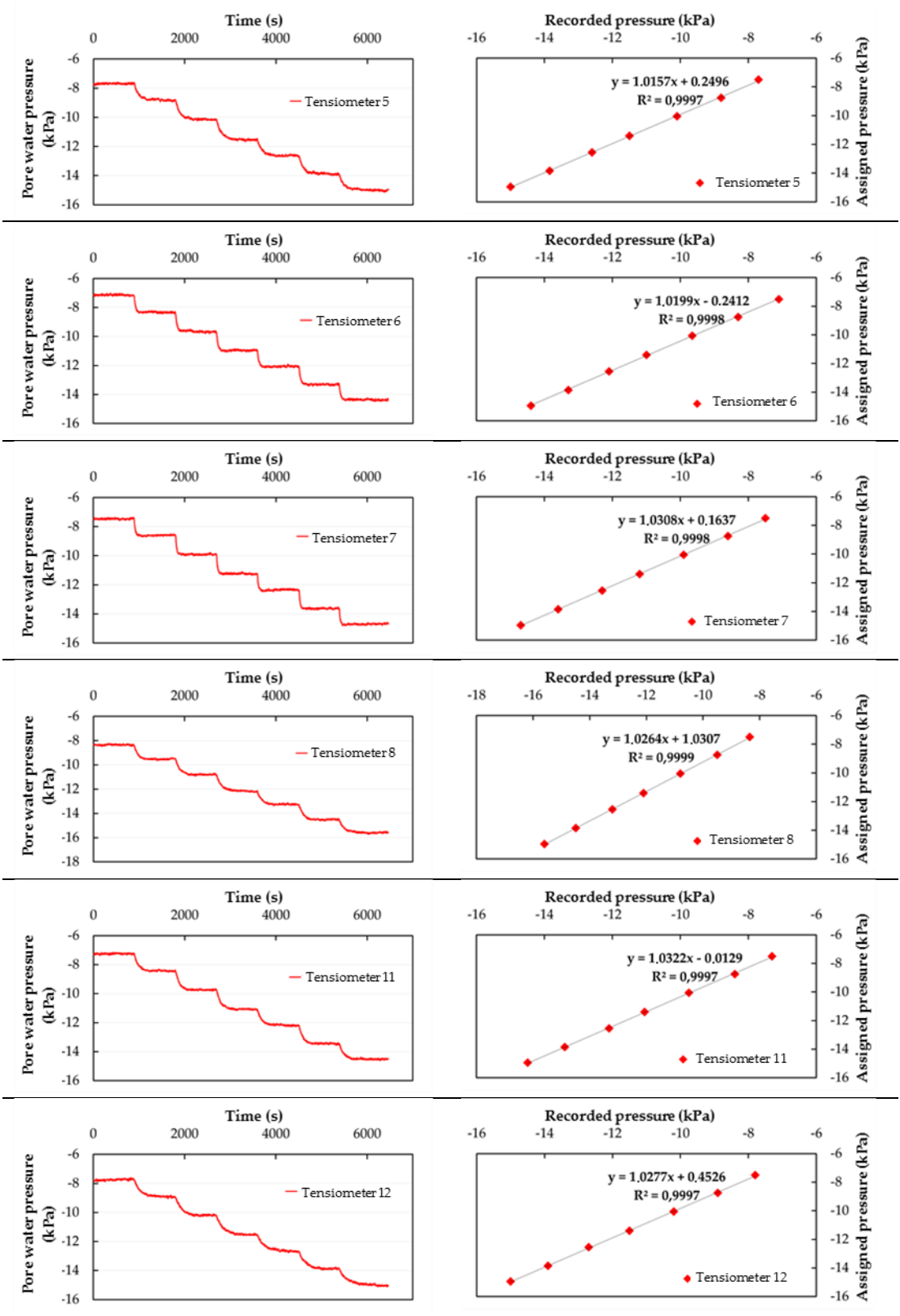

Figure 25: Right-hand graphs - Correlation between suction values applied and those recorded Left-hand graphs - Values recorded by tensiometers during calibration.

2.1.2. PRESSURE TRANSDUCERS

Neutral pressure transducers installed on the flume bed have low scale base and high sensitivity so that they are able to read millimetric neutral pressures in the water column and with low response times. The transducers are lodged appropriately on the flume bed. It should be ascertained that the transducer lodgment hole is watertight, to prevent any water head from dissipating. It is then verified that water drops do not form below the transducers. If so, any cracks are sealed with silicon rubber. Since the devices, once they have been activated, may experience negative thermal effects in relation to the heating of circuits, transducers should be charged and activated several hours prior to use.

2.1.2.1. TRANSDUCER CALIBRATION

The instruments are calibrated by applying above the load cell a water column of known height and by recording the output signal from the sensor once it has stabilized. By then varying the height of the water column several times and repeating the measurements the calibration correlation is identified. Similar to what is described for tensiometers, also in this case the calibration procedure allows the instrument's precision and response time to be verified. The way in which pressure was applied to instruments is shown in Figure 26.

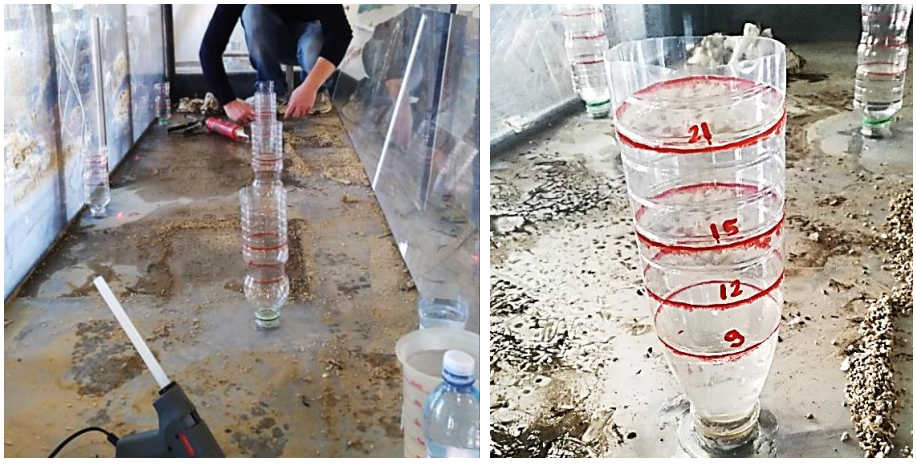

Figure 26: Containers placed on pressure transducers for calibration.

Some containers with heights marked were arranged above the load cells, fixing them with hot glue and silicon to ensure airtightness. Measurements were then taken on each, filling the containers to the various levels indicated. Attention was paid during the sensor immersion phase so that air did not remain trapped inside the measurement chamber. It was felt appropriate that the system, prior to the calibration procedure, be left charged for several days in an environment with controlled temperature and humidity, to prevent instrument drift, and to dissolve in water any remaining air trapped in the measurement chamber. The graphics in Figure 27 refer to the load phase which lasted about five days.

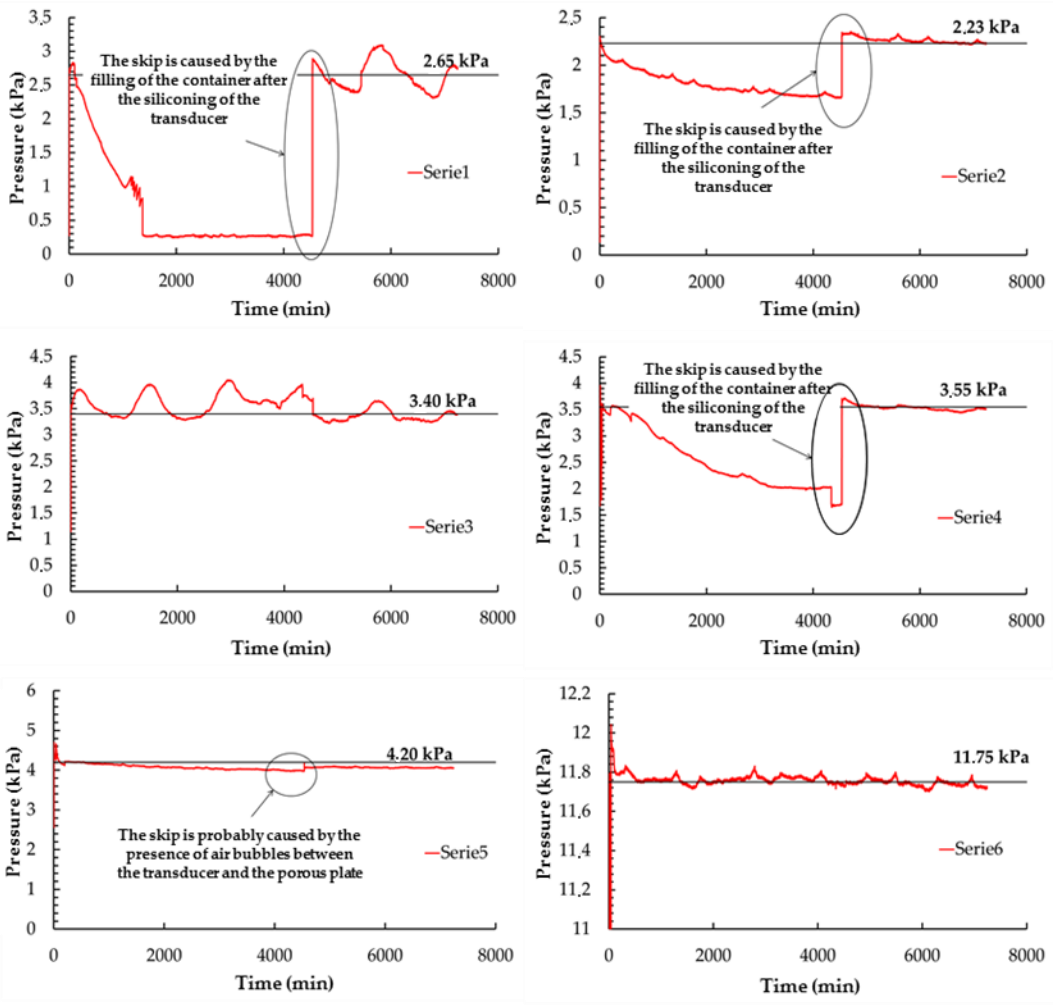

Figure 27: Loading phase of the pressure transducers.

As may be inferred from the graphs, transducers 1-2-4 were not installed in a watertight manner. The water dripped from the bottom of the transducers and the water level inside the containers decreased. After three days silicon was used to seal the bottom of the transducers and the water level inside the containers was restored. As may be noted from the graphs, this intervention prevented further leakage of liquid.

Once certain of the system's stability, we proceed to impose on the sensors some water column heights and record the relative values. In Figure 28 the values recorded during the calibration phase are plotted.

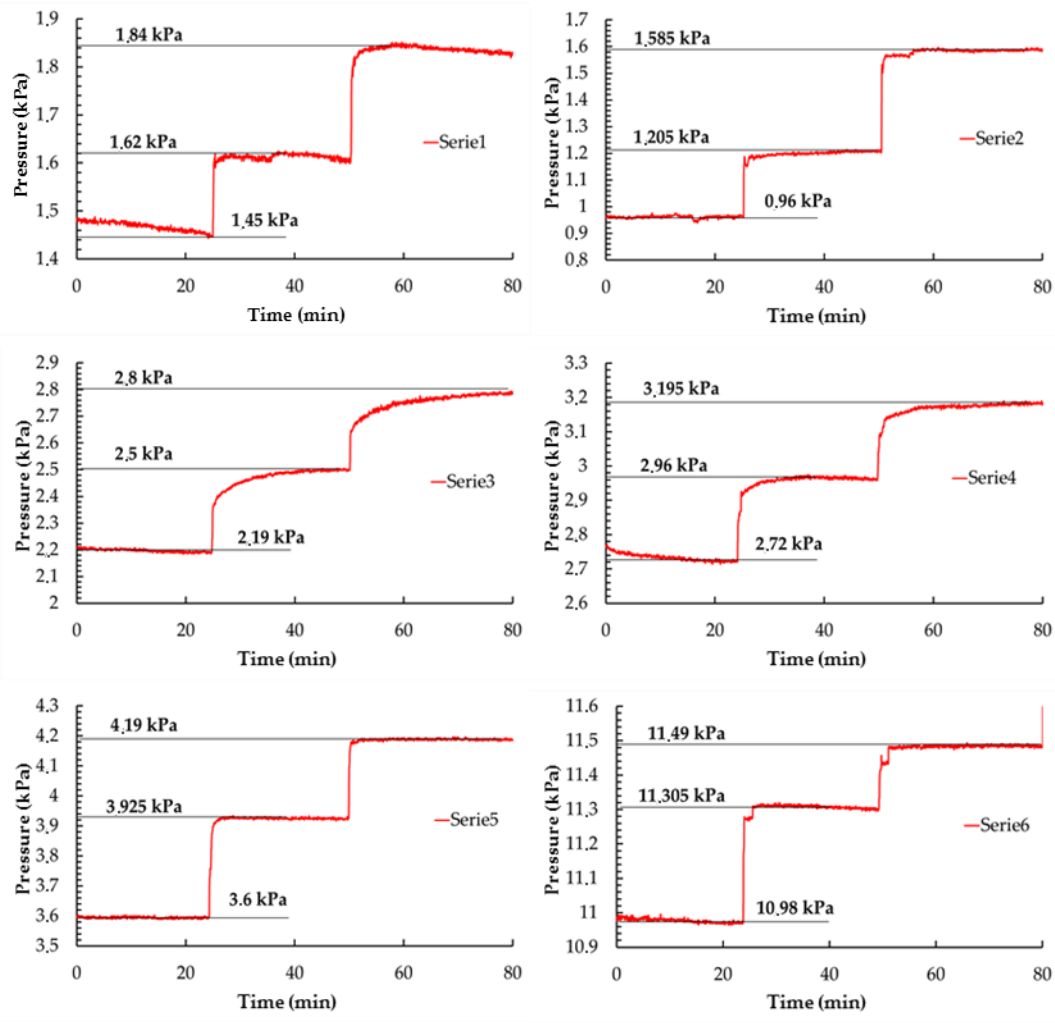

Figure 28: Values recorded during the calibration phase.

From the graphs it may be noted that almost all the transducers have an almost immediate response to the load increase except for transducer 3 which takes more time to stabilize. Using all the pairs of values (applied and recorded), the calibration curves of the transducers were constructed (Figure 29).

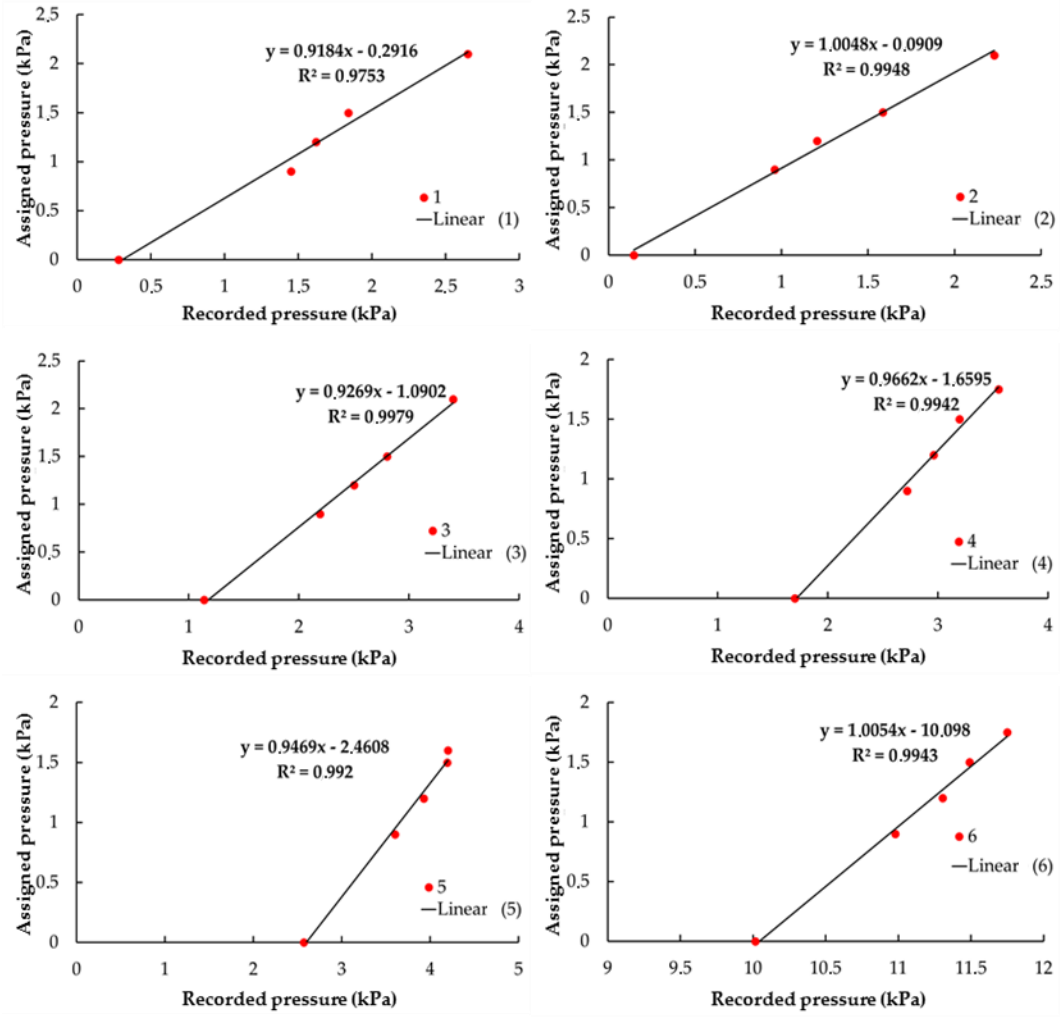

Figure 29: Calibration curves of the pressure transducers.

Table 6 reports the loads applied with the respective data recorded by the transducers.

Load applied		Pressure recorded by transducers					
cm	kPa	Trasd. 1 [kPa]	Trasd. 2 [kPa]	Trasd. 3 [kPa]	Trasd. 4 [kPa]	Trasd. 5 [kPa]	Trasd. 6 [kPa]
0	0	0.28	0.145	1.14	1.7	2.57	10.015
9	0.9	1.45	0.96	2.19	2.72	3.6	10.98
12	1.2	1.62	1.205	2.5	2.96	3.925	11.305
15	1.5	1.84	1.585	2.8	3.195	4.19	11.49
16	1.6	-	-	-	-	4.2	-
17.5	1.75	-	-	-	3.55	-	11.75
21	2.1	2.65	2.23	3.4	-	-	-

Table 6: Correspondence between loads applied and loads recorded by transducers during calibration.

2.1.3. DISPLACEMENT TRANSDUCERS

The vertical displacements of the soil surface are measured with laser displacement transducers for contact-free measurements. The transducers used do not require metal targets. They use the principle of optical triangulation by projecting a modulated light onto a fixed lens and are equipped with sensors (CCDarray) able to measure diffuse light intensity reflected and transmitted to the sensor by a focusing lens which is sloping in relation to the optical axis of the laser. The operative temperature field is between 0 and 55°C.

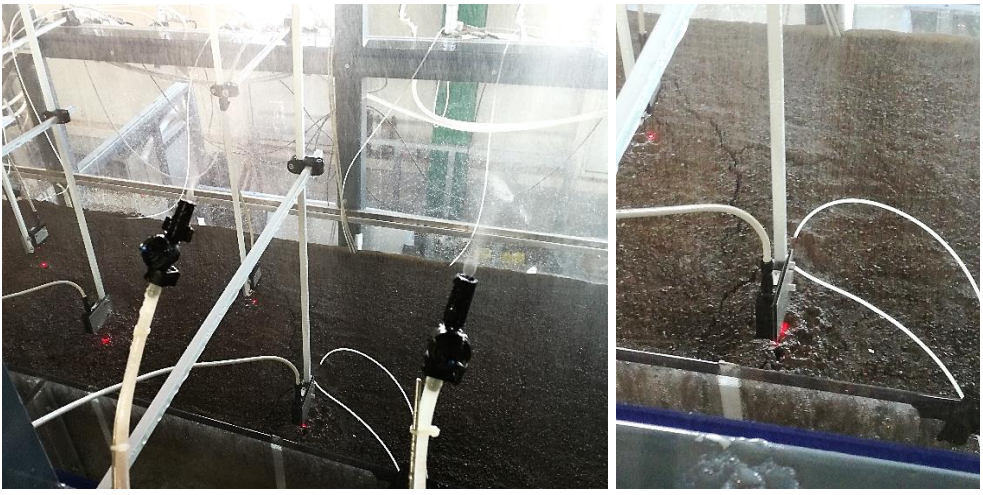

Figure 30: Arrangement of laser sensors during a rainfall phase.

The instruments should be arranged with the optical axis perpendicular to the surface to be monitored (Figure 30). Deviations of between 5° and 15° correspond to distance calculation errors of about 0.5% of the field of measurement, which increase to 1% for deviations between 15° and 30°.
The surface roughness of the deposit obviously leads to a background noise in the response of the instrument which is nevertheless tolerable in the current applications, insofar as it is about one-tenth of a millimeter. The sensors have to be charged about 30 minutes before the test begins to obtain a uniform temperature distribution inside the sensor, avoiding measurement errors. The calibration constant of the instrument is supplied by the producer.

2.1.4. TDR

The instrumentation supporting the technique of Time Domain Reflectometry (TDR) consists of a generator of rectangular pulses, an oscilloscope and probes with metal rods (electrodes) to be inserted into the ground, connected to coaxial cables.
To determine the volumetric water content, a steep-fronted electromagnetic wave is propagated and its propagation time is measured (t). Once we know the time taken by the wave to propagate in the soil (t) and the length of the TDR probe (L), the propagation velocity may be defined:

$$V_p = \left(\frac{2L}{t}\right) \tag{2}$$

Having calculated V_p, it is possible to determine the dielectric constant of the soil by using equation (3) obtained by transmission line theory (Kraus and Fleisch, 1999), where c is the velocity of light in void:

$$\varepsilon_r = \left(\frac{c}{V_p}\right)^2 \tag{3}$$

Thus the technique requires a procedure to define the propagation time of the generated signal or, vice versa, its propagation velocity.

2.1.4.1. EVALUATION OF THE WAVE FORM AND CALCULATION OF THE OFFSET OF TDR PROBES

To determine the propagation velocity of the signal, a generic transmission line recorded by the oscilloscope is analyzed (Figure 31). On the wave track three points may be identified: point A, for the variation in impedance between the probe cable and handle; point B, which identifies the transit of the wave from the handle to the electrodes; point C, which represents the reflection at the open circuit.

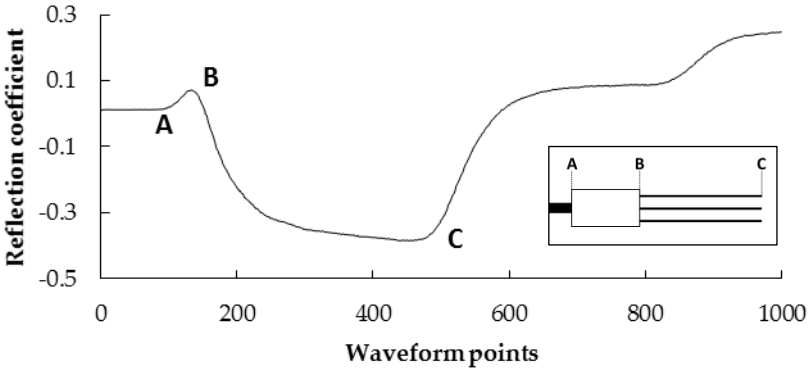

Figure 31: Typical wave form recorded with the TDR technique.

The length BC, proportional to the transit time of the signal in the soil and to the apparent dielectric constant, may be converted into equivalent distance (L_a) by using a relative propagation velocity (v), set on the TDR device. In practice, the following relations are used:

$$\sqrt{\varepsilon_r} = \frac{c}{v}; v = \frac{2L}{t_{BC}} \tag{4}$$

from which we obtain equation (5), where the electric length of the probes recorded by the TDR L_a is equal to $c \cdot t_{BC}/2$:

$$\varepsilon_r = \left(\frac{L_a}{L}\right)^2 \tag{5}$$

In the analysis of the wave track the following values therefore have to be determined: the boundaries of the reflections, points B and C, the transit time of the pulse and the length BC. The instrumentation used allows it to be

identified automatically by using a method of numerical differentiation. The track measured is smoothed numerically and the first derivative is calculated. To identify point A, a line tangent to the inflection point is drawn, coinciding with the peak of the derived curve, intersected by a line tangent to the curve in the initial section. In the same way, to determine point C a line tangent to the second inflection point of the second ascending curve is drawn, the peak of the derived curve, intersected by a line tangent to the curve (Figures 32-33). Instead, the position of B depends on the type of probe used and is generally identified by the peak after the first steep rise of the signal. To define the position of this point rigorously, we may use the approach proposed by Heimovaara (1993). The criterion consists in carrying out two measurements by placing the probe in water and air and in identifying the starting and finishing points of reflection with the method of tangents. The starting point thereby identified does not refer to the contact of the rods with the body of the probe, but concerns the change in impedance recorded in the passing of the wave from the cable to the handle. Since we know the dielectric constant of the water (ε_r=80) and air (ε_r=1), it is possible to determine the respective wave propagation times and hence the respective equivalent lengths (equation 6).

$$t = 2L\sqrt{\varepsilon_r}/c; \qquad L_a = c \cdot t/2 \tag{6}$$

An "offset" (section AB) is thus identified, to be subtracted from the total length of the reflection (section AC), so as to have the same width as the calculated equivalent (section BC).

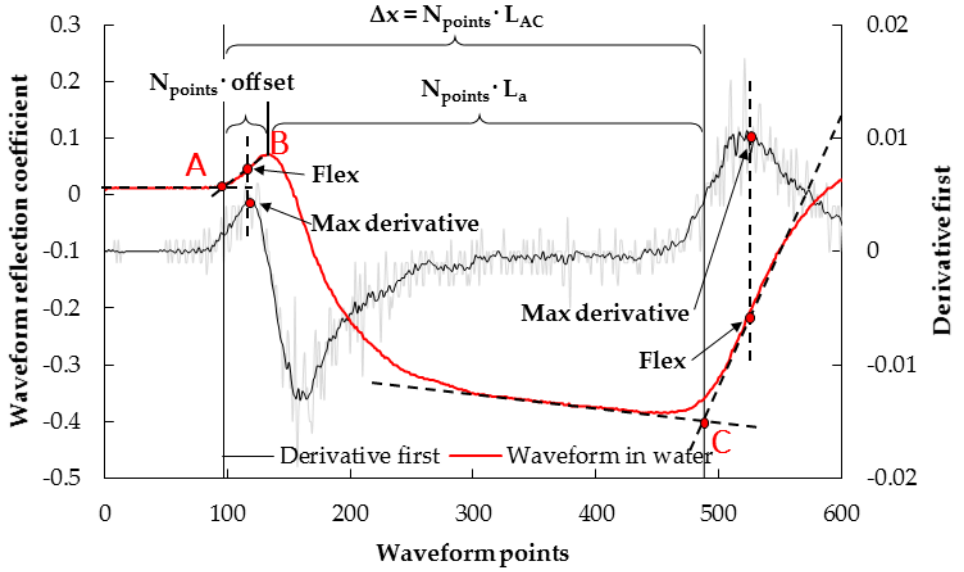

Figure 32: Wave form with the probe in water and identification of the apparent length.

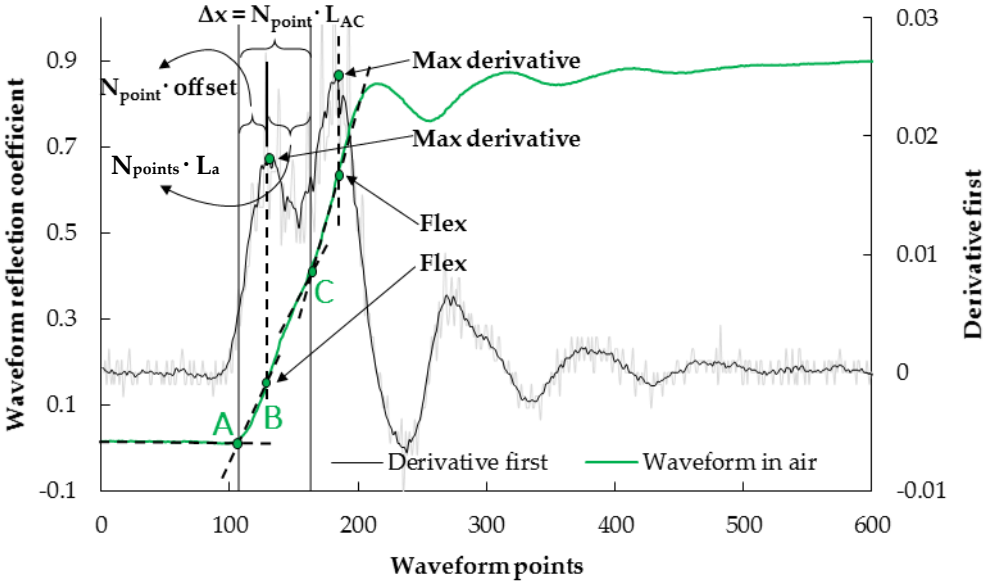

Figure 33: Wave form with the probe in air and identification of the apparent length.

This procedure, which allows the characteristic offset of the instrument to be determined, is fundamental to achieve correct calibration of the probes and hence correct evaluation of the quantities to be estimated. Below are the graphs used to determine the offset of the laboratory-made probes (Figure 34).

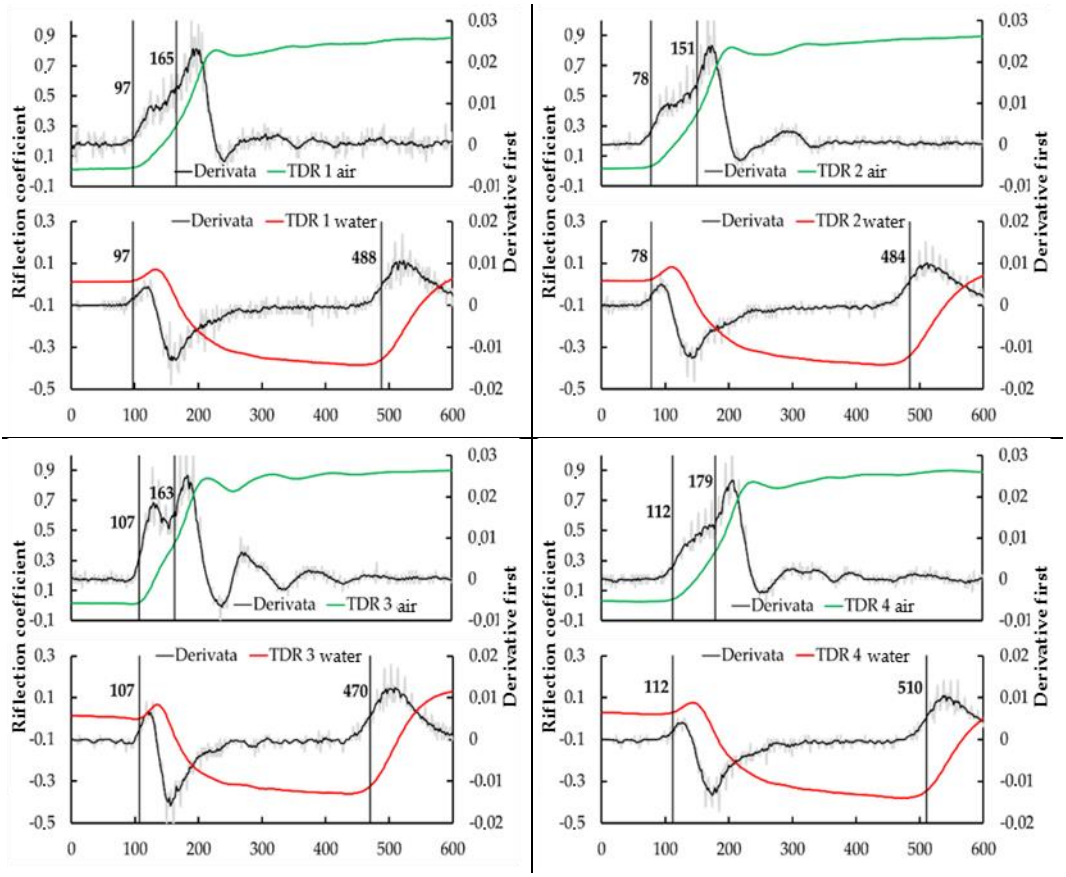

Figure 34 (first part): calculation of the apparent length for all TDR probes.

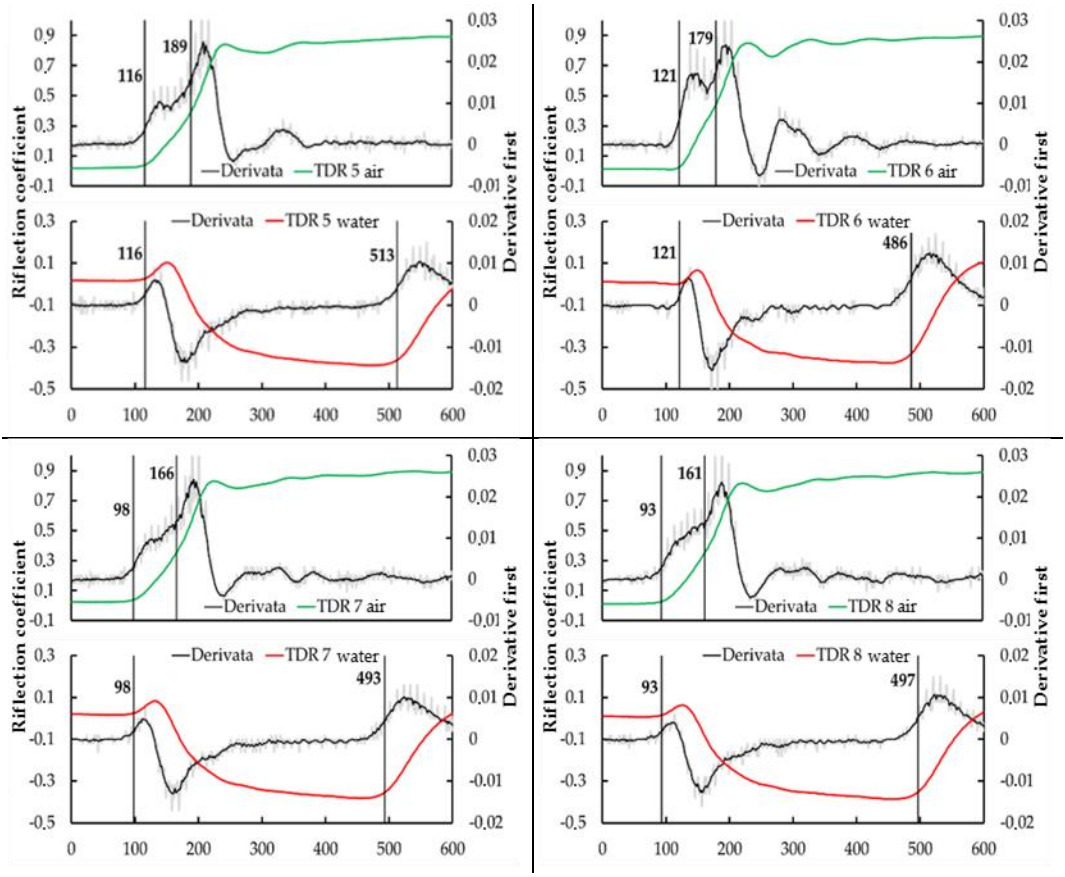

Figure 34 (second part): calculation of the apparent length for all TDR probes.

PART 3

3. EXPERIMENTATION: EXAMPLES OF FLUME USE

3.1. PRELIMINARY OPERATIONS PRIOR TO LAYING THE SOIL

The deposit in the flume is reconstituted by using the moist-tamping technique which allows higher soil porosities to be obtained than those which may be achieved with the technique of dry deposition. This is of particular importance when an experiment is to be conducted on soils with very high *in situ* porosities which are to be reproduced at a reduced scale in the test.

Some preliminary operations are necessary before being able to reconstitute the deposit. The material, taken *in situ* at a water content that may vary considerably depending on the environmental conditions in which the sample is taken, is brought to the pre-established water content either through a natural drying process, or by adding water sprayed onto the ground and subsequent mixing (Figure 35a).

Figure 35: a) Wetting and remixing of soil to bring it to a predetermined water content. b) Sieving operations.

After being sieved so as to remove roots, coarse material and other inclusions, the material is placed in hermetic containers (Figure 35b). After waiting at least 24h, enough to obtain a homogenization of the mixture, the water content is measured. The procedure is repeated until the predetermined water content is reached. At this point the soil remains closed within hermetic containers until it is used during the laying phase. Schematically:

- the impermeable sheath or the draining net is selected and placed on the flume bed (according to the type of hydraulic boundary condition to be imposed), making sure that the housing holes of the neutral pressure transducers are left uncovered (Figure 36a);
- the support is selected at the foot to the deposit, with a height corresponding to the thickness of the soil to be laid and is positioned in the housing guides appropriately arranged along the side walls of the flume (Figure 36b);
- it is verified that the water tanks are full for reproducing artificial rainfall that the water sprinkler system is working properly. Distilled water should be used to avoid the formation of calcareous encrustations in the hydraulic circuit, especially inside the nozzles for the supply of water;
- graded steps are set along the side wall of the flume, spaced about 20 cm apart, to be used as an aid for the correct laying and leveling of the soil layers.

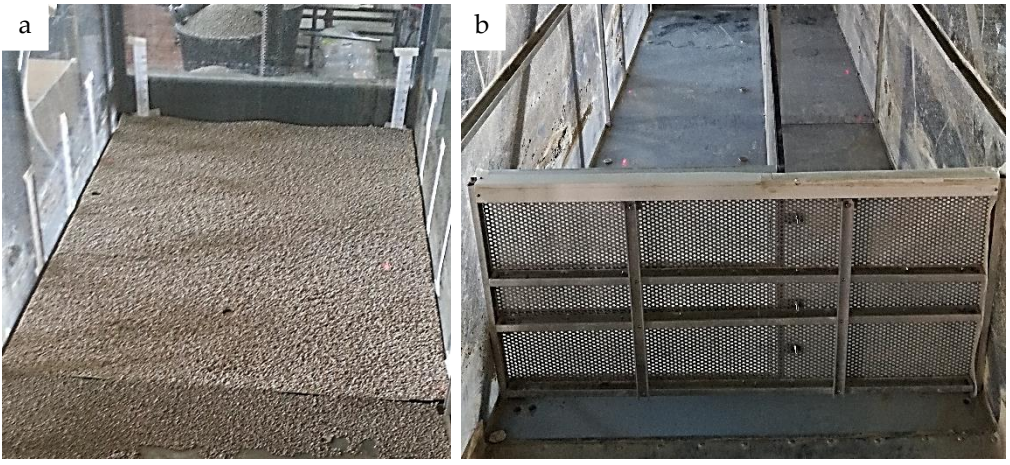

Figure 36: a) Laying of the impermeable sheath. b) Support placed at the foot.

3.2. DEPOSIT RECONSTITUTION

Reconstitution of the deposit occurs with the flume in a horizontal position. The soil is laid, with the aid of a spatula, in 2 cm thick layers so as to avoid the formation of dishomogeneous zones, verifying each time the weight of material used for each layer so as to control the value of the porosity obtained. Hence it is suitable, for each layer of material in place, to take a small soil sample to determine its water content. Should the set weight of material to be laid occupy a greater volume than that corresponding to the porosity assigned, a slight compaction of the layer is brought about until the desired height is reached.

During the reconstitution phase of the deposit, having reached the established height, the TDR probes are placed gently onto the soil surface (Figure 37a), being careful to mark their position so as not to tread on them when covered and when the soil deposit has been reconstituted. Once the soil has been laid the laser sensors and tensiometers are placed in position, following their maintenance and calibration, by pushing the porous cap inside the soil perpendicular to the deposit surface up to a set depth.

Figure 37: a) reconstruction of the deposit by layer, with the TDR probe placed in position; b) installation of the porous caps of the tensiometers.

After the insertion of the porous plate the cavity which forms between the tensiometer tube (which has a smaller diameter than that of the plate) and the surrounding soil needs to be filled with soil to avoid the creation of preferential paths of water infiltration (Figure 37b).
A low-intensity rainfall is reproduced (20-30mm/h) for 2-4 min (the duration depends on the thickness of the deposit; Figure 38a). At the end of the process the deposit is sealed with plastic sheet (Figure 38b) to avoid evaporation occurring during the water potential redistribution phase which would prevent a condition of equilibrium from being reached. The whole phase of suction equalization is monitored by the tensiometer readings. In general, 48-72 hours are sufficient to obtain the redistribution and homogenization of the water content inside the soil deposit.
At the end of the suction equalization phase, the laser displacement transducers are placed on the soil surface as well as the rain gauges. Should a test need to be carried out on the model slope, the flume is tilted until it reaches the predetermined slope.

Figure 38: a) Low-intensity rainfall phase with the deposit in a horizontal position. b) Deposit covered by a plastic sheet.

In the latter case, after inclining the flume, time is required for the deposit to reach a new equilibrium condition (usually more than 24h). The working order of all the instruments is then verified, as is the storage space available on the acquisition PC.

3.3. PERFORMANCE OF AN INFILTRATION TEST

Slope applied, prior to carrying out a test, the impermeable sheet covering the deposit is removed and data acquisition programs are started, verifying their settings (Figure 39).

The sensors are connected to the electrical system at least 30 minutes before the test begins. A test notebook is drawn up to report the initial geometric and physical characteristics of the model, the exact location of the measuring tools, the boundary conditions imposed, the name of the acquisition files and the settings used.

The test begins with reproducing rainfall of pre-established intensity. During the test the suction patterns at the various depths are monitored in real time so as to ensure that the minimum predetermined suction value is reached should it not be desirable to reach soil saturation or the approximation of a condition of complete saturation.

At the same time, the test notebook is used to record any observations on the phenomenology of the process and/or any anomalies in instrument functioning.

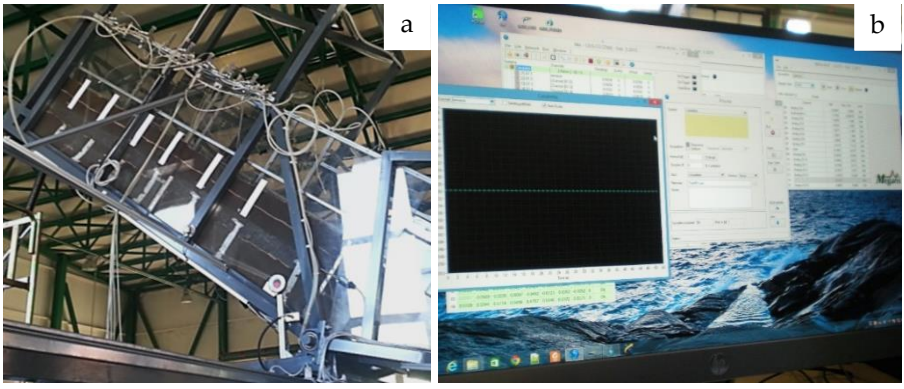

Figure 39: a) Deposit slope. b) Control of sensors and acquisition software.

3.4. HOMOGENEOUS SOIL TEST

Pyroclastic soil used for experimental tests was collected in Sarno area, South Italy, about 15 km far from the volcano Vesuvius. In May 1998, in this area, numerous and rapid mud-flows devastated the town, causing an enormous number of victims. In these places the stratigraphy are composed from limestones covered by layers of pyroclastic deposits. These soils are the product of different eruptions of more volcanoes like Somma-Vesuvius, Flegrei fields and other volcanoes present in the Region no longer active. The ashes, coming out after the eruption and carried by the wind, travel for kilometers from the eruption zone, providing a non-uniform stratigraphy for the entire area (Del Prete et al., 1998; De Vita et al., 2006; Cascini et al., 2008). Generally they are incoherent deposits with variable granulometry that range from sands, silty sands and silts (ashes) until sands with gravel (pumice) and gravels. An homogeneous deposit of pyroclastic ash was reconstructed inside the flume test, and this soil is attributable to the Plinian eruption of "Pollena" of 472 B.C.

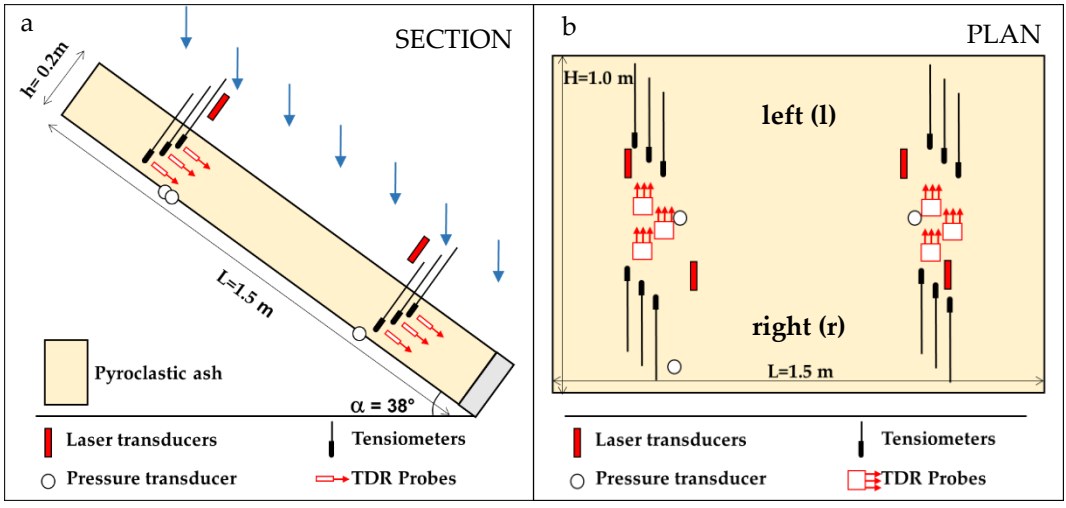

Figure 40: a) Position of the sensors in section. b) Position of the sensors (plan).

A homogeneous deposit was reconstructed inside the flume. The slope was formed by a layer of volcanic ash 20 cm thick, occupied the entire width of the flume (100 cm) and was 150 cm long. This geometry allows the deposit to be assimilated to an indefinite slope. At the base of the model there was an impervious rough bed to simulate conditions similar to those of a natural slope. At the foot of the slope a geotextile-coated drainage grid was placed.
The ash in question was sieved with a 0.4 cm mesh to eliminate coarse contamination occurring during the sampling phase. The artificial slope was re-constituted inside the flume by layers, with the moist-tamping technique, with volcanic ash porosity of between 68% and 76%, typical in situ conditions. The volumetric water content of the ash (θ) was about 20%. Inside the artificial slope, 12 tensiometers were installed to measure suction, and six TDR probes to measure volumetric water content. The sensors were installed at depths of 5 cm, 11 cm and 17 cm below ground surface, both in the upslope and downslope zone of the deposit.
On the flume bed three neutral pressure transducers were arranged, while four laser displacement transducers were installed to measure displacements perpendicular to the slope surface. Figure 40 shows schematically the location of the sensors installed inside the deposit.
Rainfall was generated with a sprinkler system placed about 100 cm above the sliding surface. The nozzles were arranged so as to ensure rainfall uniformity and avoid surface erosion.
Various tests were carried out:

1) The first was conducted with the deposit in a horizontal position. Constant rainfall of considerable intensity was simulated (about 220 mm/h) which continued for about 50 minutes[3]. The test was performed to activate infiltration phenomena so as to stabilize the slope before tilting it.
2) The deposit was then left under natural evaporation for about 14 days, acquiring the values recorded by the various sensors.
3) The slope was then inclined at 38°, leaving it in evaporation for about 8 days, so as to redistribute the suction values and water content in the new configuration.

[3] This test was carried out while a first version of the rain system was installed that allowed rains of greater intensity.

4) Finally, a new infiltration phase was simulated, with constant rainfall at an intensity of about 220 mm/h, which lasted until slope failure (about 40 minutes).

The main characteristics of the various test phases are summarized in Table 7.

Test	Inclination angle (degrees)	Rainfall intensity (mm/h)	Duration
Horizontal deposit infiltration	0	220	50 minutes
Evaporation	0	0	14 days
Redistribution	38	0	8 days
Failure	38	220	40 minutes

Table 7: Main characteristics of the various test phases.

3.4.1. TEST RESULTS

During the various tests, values of suction and volumetric water content were acquired both in the upslope and downslope zones at different depths. Displacements perpendicular to the slope surface were also measured, produced by the variation in the tension state, and the water pressure on the flume bed. Acquisition frequency varied according to the type of test. During the phases which envisaged the simulation of rainfall and the relative infiltration of water into the soil, since the monitored values varied rapidly, the acquisition frequency was in the order of seconds. By contrast, during the evaporation phases, the variations were decidedly slower. Hence it was resolved to acquire values with hourly intervals. The main results of the various test phases are reported below.

3.4.1.1. INFILTRATION PHASE IN A HORIZONTAL DEPOSIT

With the deposit in a horizontal position, rainfall of considerable intensity was simulated (about 220 mm/h). During this phase all the major dimensions were monitored. Figure 41 reports the pattern of matric suction in time. As may be observed from the graph, the suction values recorded prior to rainfall were very heterogeneous. This great dishomogeneity of values may well have been due to the non-perfect adherence of the porous plates of the tensiometers to the soil. During the sensor installation phase, the porous plates and the tubes connected to them were inserted inside appropriately arranged holes. After installation, the holes were filled, although there was no certainty of the soil

adhering to the plates. Any voids that were created close to the porous plates were subsequently filled due to the effect of infiltration processes which were generated after the simulated rainfall. Figure 41 shows that suction values after rainfall, following a settlement phase, all converge on the same values.

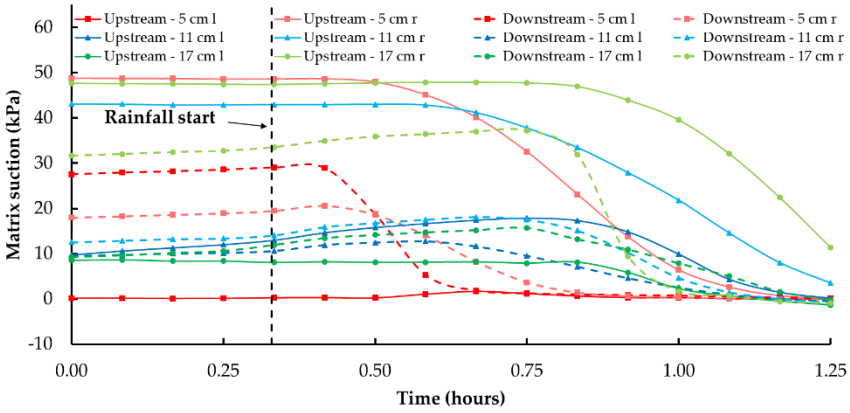

Figure 41: Suction time course during the first phase.

Figure 42 shows the pattern of neutral pressures recorded by pressure transducers on the flume bed, while Figure 43 reports the pattern of volumetric soil water content, detected through six TDR probes. The TDR measurements were processed by using a calibration equation specifically obtained for volcanic ash coming from the slope of Cervinara (AV), originating from the same volcanic eruption responsible for the pyroclastic deposits at Sarno, of similar physical and mineralogical properties to those of the soil used to make the deposit in the flume (Greco and Guida, 2010).

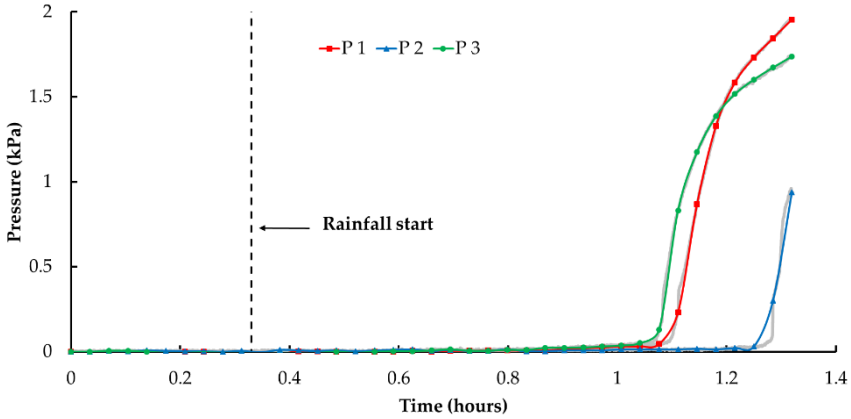

Figure 42: Time course of water pressure recorded by pressure transducers on the flume bed during the first phase.

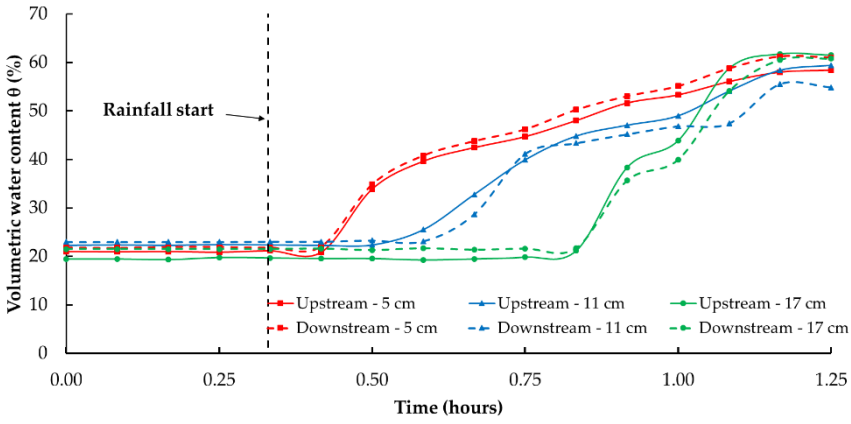

Figure 43: Time course of volumetric water content recorded by TDR system during the first phase.

As may be inferred from Figure 43, the initial volumetric water content, recorded at various depths, appears substantially homogeneous. This configuration ensured that the wetting front advanced vertically homogeneously. Both the neutral pressure transducers place on the flume bed and most of the tensiometers showed that almost the whole deposit reached conditions of complete saturation. Values of volumetric water content show that at the end of the test the porosity of the deposit was about 60%, indicating a rather compacted condition for the type of soil in question (NB: in the field porosities of around 75% are frequently observed). This value should come as no surprise, seeing that very loose pyroclastic soils show, when wetted up to

conditions close to saturation, the phenomenon of volumetric collapse: under the sole action of tension states deriving from their own weight, they undergo a considerable reduction in volume. The emergence of this phenomenon during the infiltration phase in the flume is attested by Figure 44, which reports the pattern of displacements experienced by the ground surface during the test, measured by laser transducers.

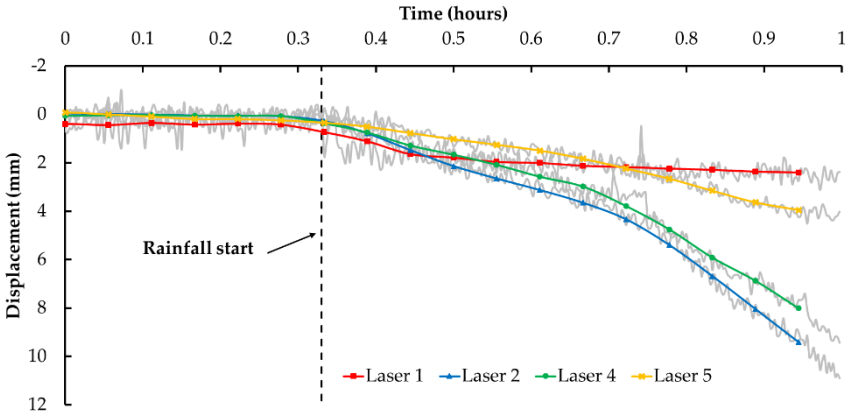

Figure 44: Time course of displacements experienced by the ground surface during the experiment.

As shown by Figure 44, the soil surface is lowered by several centimeters. The displacement interval ranged from about 2 cm recorded by laser L1 to little more than 1 cm recorded by laser L2. Given the initial thickness of the deposit of about 20 cm, this lowering corresponds to a decrease in porosity, compared with the initial value, of several percentage points (up to around 5% at transducers L2 and L4).

3.4.1.2. EVAPORATION PHASE IN THE HORIZONTAL DEPOSIT

At the end of the infiltration phase, the deposit was left in natural evaporation. This phase lasted about two weeks insofar as the environmental conditions inside the laboratory (high relative air humidity) produced a very slow evaporative process. Figure 45 shows the pattern of suction recorded by the various tensiometers inside the deposit. It may be inferred from the graph that, after a brief initial phase of rapid suction increase, the phenomenon evolved extremely slowly. The graph also shows the variation in suction obtained in the alternation of day and night. At the end of this phase, suction

values between 2 kPa (recorded by the deeper probes) and 5 kPa (recorded by probes closer to the surface) were detected.

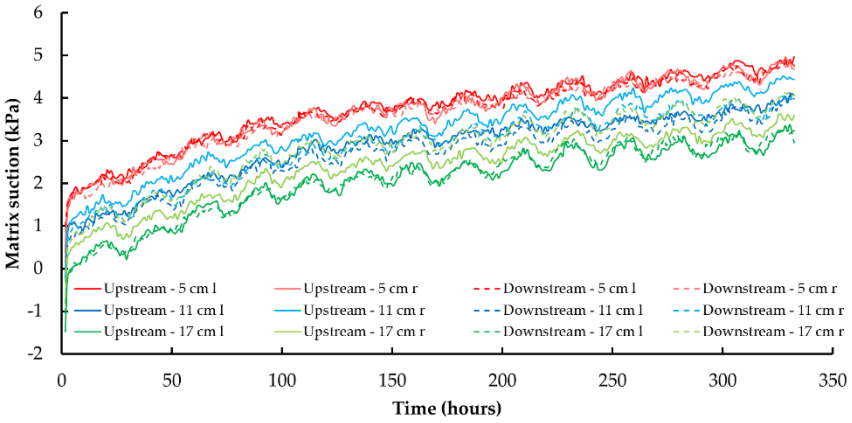

Figure 45: Suction plotted against time in the second phase.

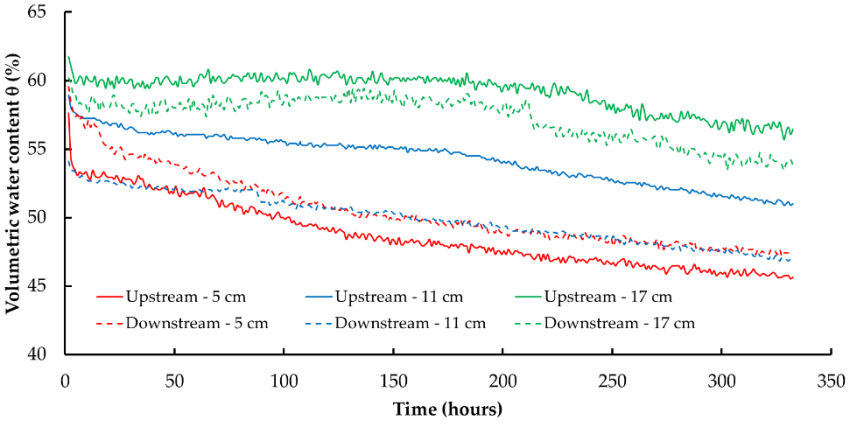

Figure 46: Volumetric water content vs. time in the second phase.

The trend in volumetric water content recorded by TDR during the evaporation phase is shown in Figure 46. After a brief initial phase of rapid decrease in water content there emerges a slow evolution of the phenomenon. At the end of the test, volumetric water content values were between 45% and 57%. The relative breadth of the range of conductivity values, compared with the much narrower range of suction values, indicates that the water retention curves of the soil in question rise extremely sharply close to saturation, a characteristic typical of coarse-grained soils, which ensures that small

variations in capillary pressure are matched by large variations in water content.

The patterns of values supplied by the probes placed lower down show that the evaporative flow took over a week to significantly affect also the deeper part of the deposit.

3.4.1.3. REDISTRIBUTION PHASE IN A SLOPING DEPOSIT

When the suction recorded inside the deposit settled on values between 3kPa and 5kPa, representing conditions such as to permit the soil to easily withstand application of a significant increase in shear stress, the slope was then tilted up to an angle of about 38°. The action of gravity, following changes in height, triggered a redistribution of suction and volumetric water content. The whole phase lasted about eight days, but as may be noted from Figure 47, which shows the suction trend in time, there was a significant change already in the first hour. Subsequently, suction values changed slowly, a change produced by evaporation which became established in the new configuration. The figure also shows that, due to the effect of gravity, the suction values recorded by all the sensors positioned downslope are about 4 kPa lower than those upslope.

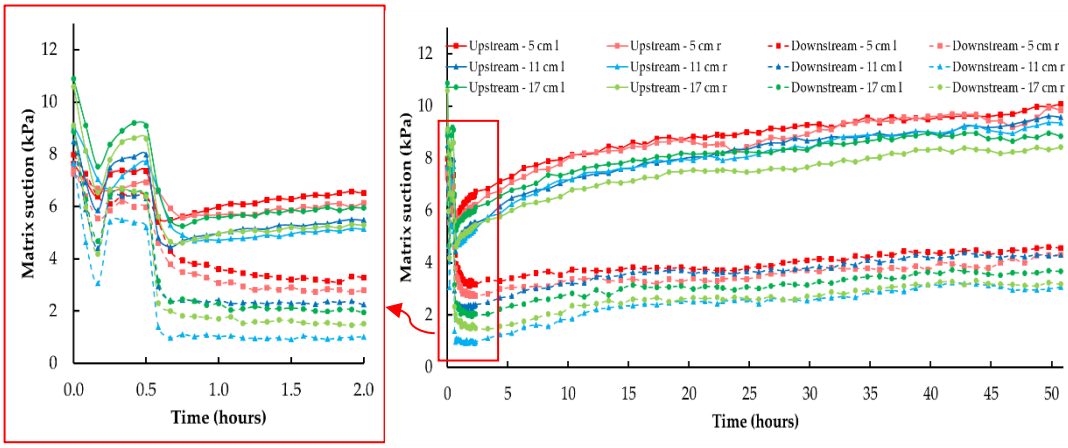

Figure 47: Suction trend in time during the third phase.

The variation of depth may also be noted by observing the trend in volumetric water content reported in Figure 48. Also in this case, after a brief transitory phase of redistribution of the volumetric water content, the values changed

slowly, a variation produced by evaporation which was established in the new configuration.

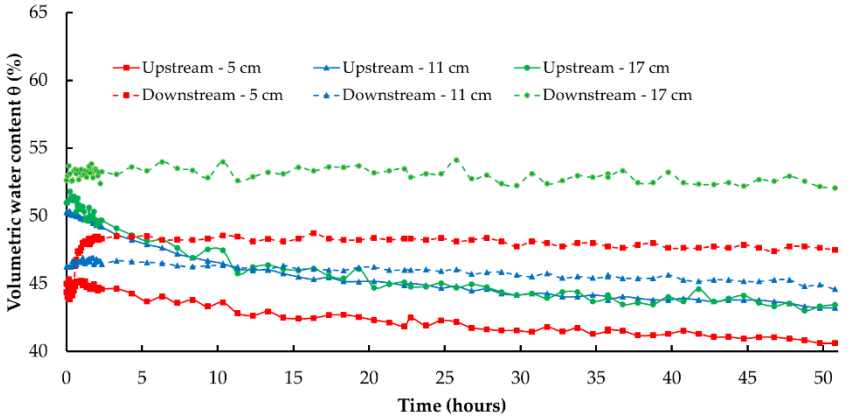

Figure 48: Volumetric water content vs. time in the third phase.

3.4.1.4. INFILTRATION PHASE IN AN INCLINED DEPOSIT

Having determined that the redistribution linked to the change in geometric configuration had been concluded, a further infiltration phase was initiated, with high-intensity artificial rainfall (about 220 mm/h), in order to reach conditions such as to trigger a landslide along the artificial slope. The suction pattern during the last infiltration phase (Figure 49) clearly shows that saturation conditions at many of the 12 tensiometers are swiftly reached (the figure, to make it more legible, reports only the values of the tensiometers installed on the right-hand side, given that the values recorded by those installed on the left showed the same trend). It is also possible to note the moment in which the curves for tensiometers placed downslope at 5 cm and 11 cm of depth have a rapid variation in slope, that is when part of the slope is detached and a small surface landslide is triggered.

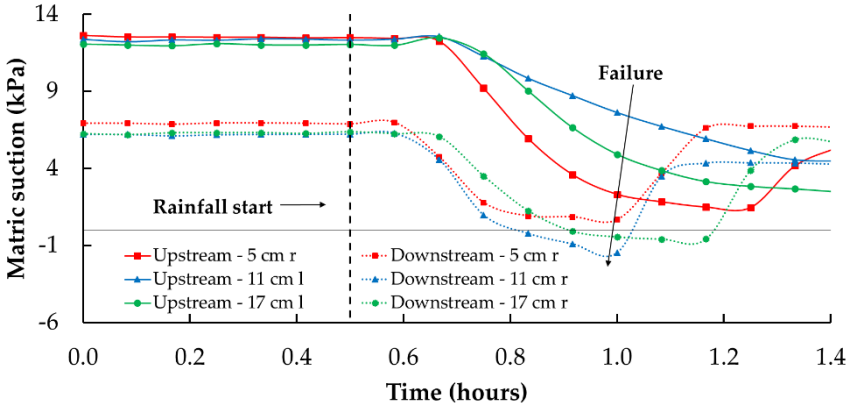

Figure 49: Time course of suction in the fourth phase.

Trends in soil volumetric water content are reported in Figure 50, measured with the six TDR probes. It appears evident, also in this phase of infiltration in a sloping channel, the progressive advancement of a wetting front from the top, although some differences are observed between the upslope and downslope zones where, perhaps due to the non-perfect homogeneity of the spatial distribution of artificial rainfall, but especially due to the sub-surface flow parallel to the slope, the increase in water content appears anticipated. It should also be pointed out that all the TDR probes, despite there being absolute evidence that much of the deposit reaches complete saturation conditions, detected water content values between 50% and 55%. This is doubtless to be attributed to compaction experienced by the deposit during the previous test phases, which had led to a reduction in width from the initial 20 cm to around 18 cm, corresponding to a estimated reduction in porosity of around 10%. This graph also shows the moment in which a small landslide is detached, producing an abrupt change in the steepness of the curve for the TDR positioned in the most superficial part downslope. In this case the landslide brought the TDR to the surface and from that point onward the values measured by the sensor are not representative of real water content.

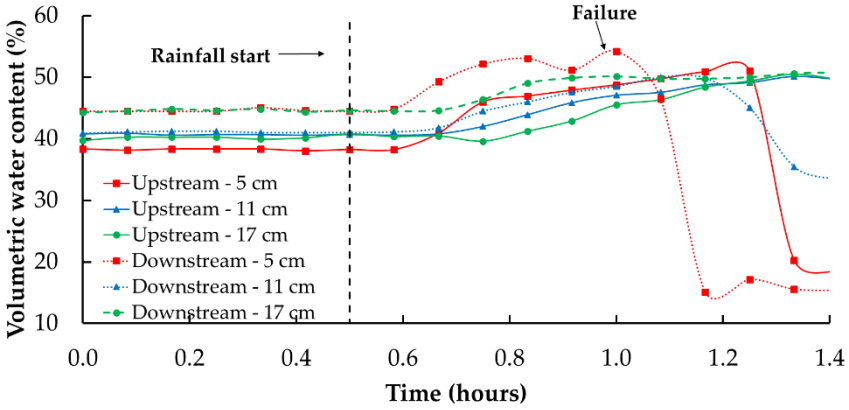

Figure 50: Volumetric water content vs. time in the fourth phase.

The time course of water pressure recorded by the pressure transducers on the flume bed is shown in Figure 51 while Figure 52 illustrates the trend in displacements perpendicular to the slope surface as recorded by laser displacement transducers. It may be observed (Figure 51) that the deposit was almost all saturated. Indeed, the transducers (except for P2) recorded an increase in pressure due to the formation of water head on the flume bed, while Figure 52 shows that during this phase, the slope swells by a few millimeters.

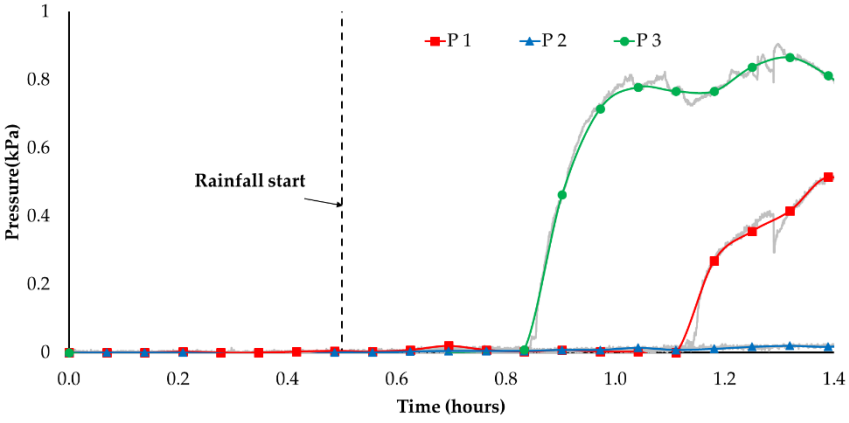

Figure 51: Trend of pressure recorded on the flume bed in the fourth phase.

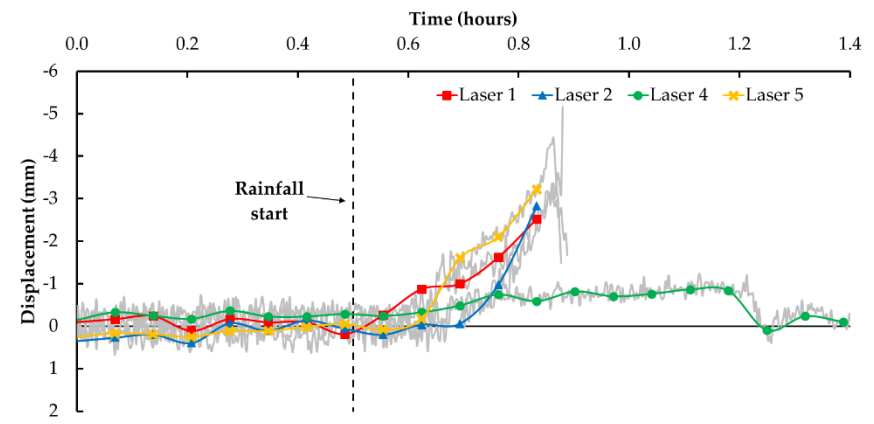

Figure 52: Trend of displacements perpendicular to the slope in the fourth phase.

Finally, in Figure 53 the appearance of the deposit at the end of the test. The figure clearly shows the detachment niche of the landslide and the eroded surface.

Figure 53: Deposit at the end of the test.

Slope failure, consistent with the compacted configuration assumed by the deposit during the previous test phases, did not trigger a mud-flow. It took the form of a progressive erosion of the more superficial soil layers, initially and chiefly concentrated in the downslope zone, where the intense sub-surface flow resulted in conditions of greater moisture being reached and, at

the same time, encouraged soil mobilization. The first local failures began to occur about 20 minutes after the beginning of artificial rainfall, and only after that did they extend so far as to affect the points in which some of the tensiometers and TDR probes had been installed.

3.5. USE OF ROCKFALL BARRIERS

As broadly described in the previous sections the model allows different configurations to be defined in relation to the objectives to be pursued. Besides the analysis of the triggering conditions and propagation in cohesive soils, the behavior of loose granular soils can also be examined via the insertion of further instruments. Installing appropriate supports on the flume (Figure 54a), it is possible to connect some rockfall barriers on a small scale (Figure 54b) and simulate the behavior of a debris flow. A debris flow consisting of aggregates of particles of known sizes may be triggered in the upper flume, modifying its initial set-up. Using this experimental configuration, different tests can be carried out by changing each time the inclination of the lower flume (thus making the propagation velocity change) or the configuration of barriers.

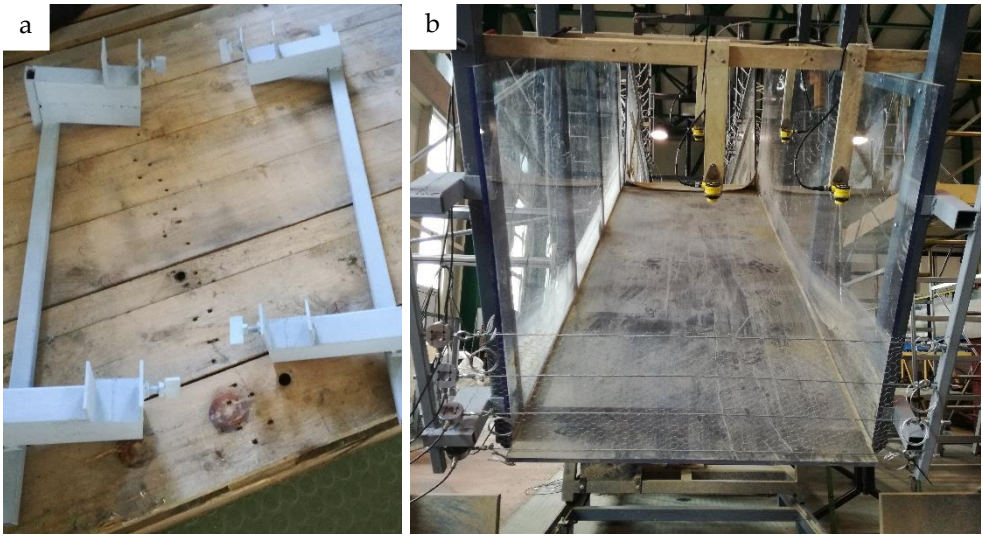

Figure 54: a) Supports for raising barriers. b) Rockfall barrier installed on the flume.

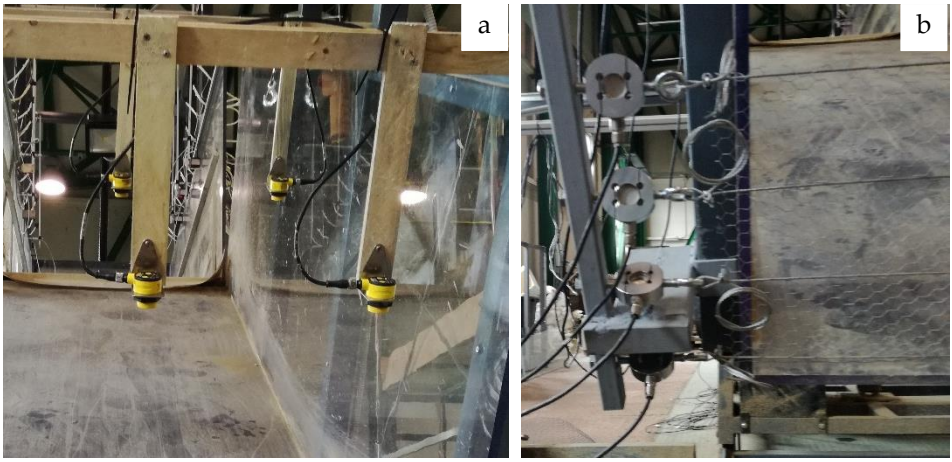

Figure 55: a) Ultrasonic altimeters. b) Load cells.

Thus, thanks the instrumentation already present and to that of the installable support, all the necessary dimensions can be identified for perfect definition of the barrier and for understanding the phenomenon. Indeed, thanks to high-resolution video cameras with dedicated PIV software the velocity attained by the flows may be determined, while through ultrasonic altimeters (Figure 55a) the height reached by the flow is identified. To complete the instrumentation a series of load cells may be installed (Figure 55b), allowing measurement of the forces present on the ropes, which form the barrier, during and after the impact with the debris flow.

Below are several images of the tests carried out on the flume in collaboration with the University of Parma, using detritic material of variable size. The various tests were performed without the influence of the rainfall event, and the trigger occurred by tilting the upper flume. Moreover, by defining an almost real stratigraphy it is also possible to analyze the effect of rainfall on these materials, thereby seeking to determine the quantities that most affect its behavior. Finally, thanks to the small-scale model, the behavior of the system of protection under the influence of such flows may be better understood, with a view to improving environmental protection and reducing the associated risk.

Figure 56: Test conducted in collaboration with the University of Parma: initial configuration.

Figure 57: Test conducted in collaboration with the University of Parma: configuration at the end of the test.

Figure 58: Test conducted in collaboration with the University of Parma: configuration of the flume at the end of the test.

REFERENCES

Bin Zhang, Chanjuan Han, Xiong (Bill) Yu, 2015. A non-destructive method to measure the thermal properties of frozen soils during phase transition. Journal of Rock Mechanics and Geotechnical Engineering; Volume 7, Issue 2, pages 155-162.

Cascini L., Cuomo S., Guida D., 2008. Typical source areas of May 1998 flow-like mass movements in the Campania region, Southern Italy. Engineering Geology 96 107–125

Dasberg, S., Dalton, F.N. Time domain reflectometry field measurement of soil water content and electrical conductivity. Soil Science Society of America Journal, 1985, 49, 293-297.

Del Prete M., Guadagno, F. M. & Hawkins, A. B., 1998. Preliminary report on the landslides of 5 May 1998, Campania, southern Italy. Bull. Engineering Geology and the Environment, vol. 57, 113-129.

De Vita P., Di Clemente E., Rolandi M. & Celico P., 2007. Engineering geological Models of the initial landislides occorre on the April 30th, 2006 at the mount di Vezzi (Ischia Island, Italy). Italian Journal of Engineering Geology an Env., 2, 119, 141.

Eckersley J.D., 1990. Instrumented laboratory flowslides. Géotechnique 40, 3, pp. 489-502.

German, P.F., Di Pietro, L., Singh, V.P. Momentum of flow in soils assessed with TDR moisture readings. Geoderma, 1997, 80, 153-168.

Greco, R. Soil water content inverse profiling from single TDR waveforms, Journal Hydrol., 2006, 317, 325-339.

Greco, R., Guida, A. Determinazione sperimentale del legame tra permettività dielettrica e contenuto d'acqua in piroclastici campane. Convegno nazionale di Idraulica e Costruzioni Idrauliche, 14 – 17 Settembre 2010, Palermo.

Iverson R.M. & LaHusen R.G., 1989. Dynamic pore pressure fluctuations in rapidly shearing granular materials. Science, 246, pp. 796-799.

Kraus J.D., Fleisch D.A., 1999. Electromagnetics with applications. McGraw-Hill.

Lacerda W.A. & Avelar A.S., 2003. Flume tests on sand subjected to seepage with the influence of hidden barriers. Proc. Int. Workshop on Occurrence and Mechanisms of Flows in Natural Slopes and Earthfills, Sorrento.

Okura Y., Ochiai H., Sammori T., 2002. Flow failure caused by monotonic liquefaction. Proc. Int. Symp. Landslide Risk Mitigation and Protection of Cultural and Natural Heritage, 21-25 January 2002, Kyoto University, Kyoto, pp. 155-172.

Olivares L., Damiano E., Greco R., Zeni L., Picarelli L., Minardo A., Guida A., Bernini R., 2009. An Instrumented Flume to Investigate the Mechanics of Rainfall-Induced Landslides in Unsaturated Granular Soils. Geotechnical Testing Journal, Vol. 32, No. 2

Spence K.J. & Guymer I., 1997. Small-scale laboratory flowslides. Géotechnique 47, 5, pp. 915-932.

Wang G. & Sassa K., 2001. Factors affecting rainfall-induced landslides in laboratory flume tests. Géotechnique 51, 7, pp. 587-599.

Topp, G.C., Davis, J.L., & Annan, A.P. Electromagnetic determination of soil water content: measurement in coaxial transmission lines, Water Resour. Res., 1980, 16, 574-582.

Zegelin S.J., White I., Russel G.F., 1992. A Critique of the Time Domain Reflectometry Technique for Determining Field Soil-Water Content. Advances in Measurement of Soil Physical Properties: Bringing Theory into Practice, SSSA Special Publication n. 30, Soil Science Society of America, Madison, WI, pp. 187-208.

Prototype made by
GISA s.r.l.
MEGARIS


Lab
CAMI
Lab. di
Cartografia
Ambientale e
Modellistica Idrogeologica
UNIVERSITÀ DELLA CALABRIA